



UNIVERSITATEA "POLITEHNICA" din BUCUREȘTI
FACULTATEA DE ȘTIINȚE APLICATE

**ADVANCED SPECTROSCOPIC TECHNIQUES
APPLIED IN THE STUDY OF
NUCLEAR STRUCTURE**

Thesis Summary

Cristian COSTACHE

PhD Coordinator
Prof. Dr. Gheorghe CĂTA-DANIL

IFIN-HH Scientific Supervisor
CS I Dr. Nicolae Marius MĂRGINEAN

Contents

1	Introduction on nuclear structure in the neutron deficient Po isotopes	1
2	A brief survey of nuclear models relevant for medium and heavy nuclei near closed shells	3
3	Gamma spectroscopy possibilities at the ROSPHERE multi-detector array	5
4	Lifetime measurements of excited nuclear states using the Recoil Distance Doppler Shift method and ROSPHERE	9
5	Nuclear lifetime measurements using the in-beam fast-timing technique at ROSPHERE	13
6	Precision fast-timing measurements in neutron-deficient Po isotopes at IFIN-HH	17
	Bibliography	31

Introduction on nuclear structure in the neutron deficient Po isotopes

For this thesis I concentrated my study on nuclear structure of the neutron deficient Polonium isotopes and for this I measured the lifetimes of excited nuclear states of the even-even $^{202,204,206}\text{Po}$ isotopes. In Fig. 1.1 the studied isotopes are presented in a small portion of the nuclide chart.

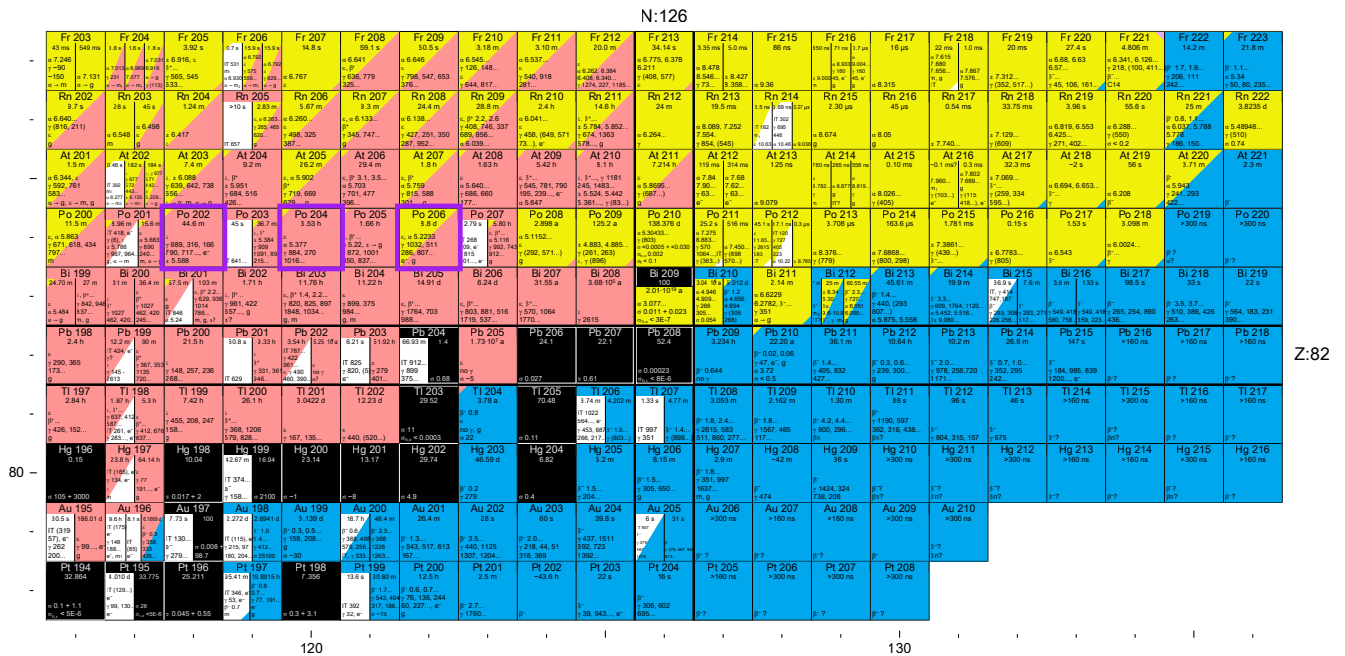


Figure 1.1: A small area of the nuclide chart centred on the double magic ^{210}Pb . The Polonium isotopes are two protons above the $Z = 82$ closed shell. The neutron deficient isotopes studied in the present thesis are marked with purple.

Polonium isotopes have $Z = 84$ and this puts them just two protons above the $Z = 82$ closed shell, with the two protons in the $1h_{9/2}$ shell. The presence of these two protons in a high angular momentum orbit ($j = 9/2$) and the proximity to the $Z = 82$ magic number make the neutron deficient Polonium isotopes good candidates for the study of the seniority regime [1] and the evolution toward nuclear collectivity as they distance from the $N = 126$ closed shell.

The 8^+ yrast states of the neutron deficient Polonium isotopes are long lived isomers while the 2^+ yrast states are short lived, with lifetimes of few picoseconds. This makes it difficult to measure the lifetimes of the 4^+ and 6^+ yrast states in the neutron deficient Polonium isotopes

and this is the main reason behind the lack of experimental data. To measure the lifetimes of the excited nuclear states of these isotopes I have used the in-beam Fast Electronic Scintillation Timing (FEST) technique [2].

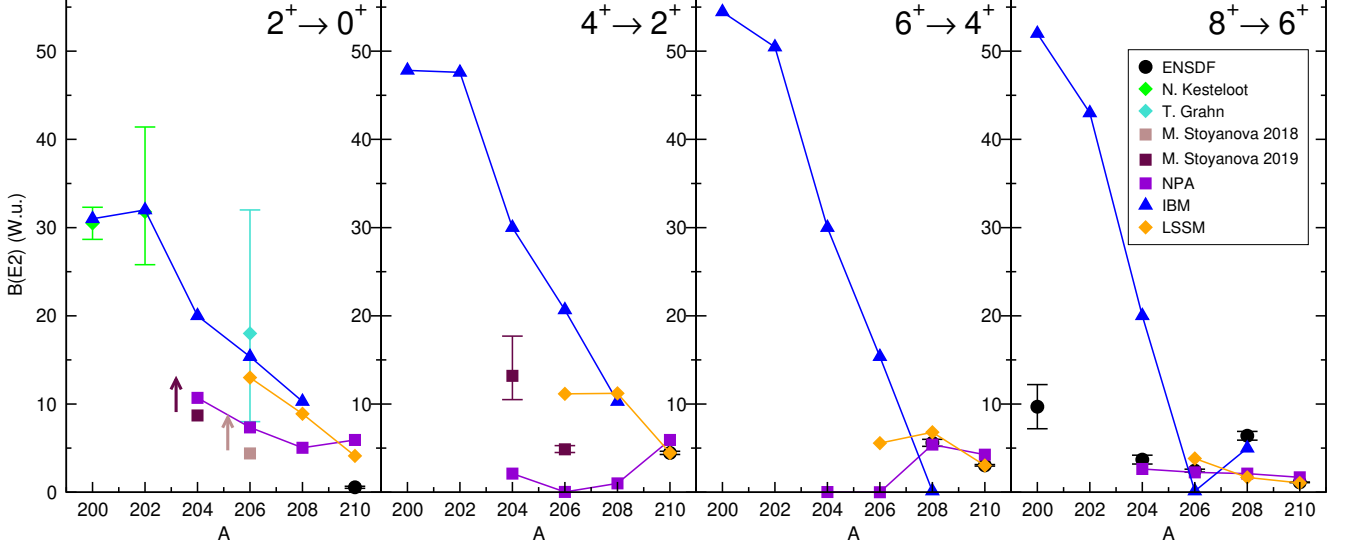


Figure 1.2: The experimental $B(E2)$ systematics [3, 4, 5, 6, 7] which connect the first yrast states in Po isotopes up to mass $A = 210$ and the recent theoretical predictions of three different models [8, 9, 10].

The available predictions of recent theoretical calculations for Polonium isotopes with $N \leq 126$ are presented against the previously known experimental data in Fig. 1.2. These values are obtained using three types of calculations, Nucleon-Pair Approximation (NPA) of the shell model [8], Interacting Boson Model (IBM) with configuration mixing [9] and Large Scale Shell Model (LSSM) calculations [10]. One can see that the predictions do not converge where there are no experimental values, while still being in good agreement with the experimental data available when the calculations were made.

The possibility to study the transition from the seniority regime to the collective motion together with the lack of experimental data together and the divergent predictions of recent theoretical calculations motivated me to do the the study on the neutron deficient Polonium isotopes presented in this paper. The experiments, the analysis and the obtained results are presented and discussed in Chapter 6.

A brief survey of nuclear models relevant for medium and heavy nuclei near closed shells

Shell Model

It became obvious, early on, in the study of the atomic nucleus that there were some nuclei which were more abundant and more stable than their neighbours [11]. They exhibited a peculiar periodicity in the proton and neutron number and it was experimentally observed that the nuclei that had both the proton number and the electron number equal to one of these values had the energy of the first excited state higher than that of neighbouring even-even nuclei. These were later called *magic numbers* [12] and their existence has led the scientist to think of a shell model of the atomic nucleus.

The usage of a realistic radial form of the potential leads to a splitting of the harmonic oscillator potential levels into $E_{nl}^{(i)}$ levels, increasing the degeneracy. A more natural shape of the potential is constructed using the spherical Woods-Saxon form factor [13]. Introducing a relatively strong spin-orbit coupling [14, 15] gives rise to a splitting of the $E_{nl}^{(i)}$ single-particle energy levels into two sub-levels with the total angular momentum $j = l \pm 1/2$ and each new level gains a $(2j + 1)$ degeneracy. The strength of the spin-orbit term increases with l and gives rise to the unnatural parity states.

The model works really well for nuclei which are close to magicity and this makes the shell model of rather limited usability. The dimension of the matrix elements for the microscopic Shell Model calculations will increase rapidly as we depart from the closed shells. The approaches used in the study of neutron deficient Polonium isotopes are the Seniority Scheme, the Nucleon-Pair Approximation, the Interacting Boson Model or the Large Scale Shell Model calculations.

Seniority Scheme

In nuclear physics the seniority number, usually noted ν , represents the number of identical nucleons that are not coupled to $J = 0$. In a pure j^2 configuration, for the ground state the pair is not broken and the two nucleons are coupled to spin-zero. For the ground state the seniority is $\nu = 0$. The pair is then broken to form the first excited level and the seniority number changes,

$\nu = 2$. For the rest of the levels the pair remains broken and the seniority number does not change ($\Delta\nu = 0$).

One feature of the seniority scheme is that the values of $B(E2)$ which connect the seniority conserving states have a downward parabolic trend across a shell. This behaviour is in contrast with the trend of the values of the $B(E2)$ than connect states with different seniority, the non-conserving transition ($\Delta\nu \neq 0$), which have an upward parabolic. Another useful feature of the seniority scheme is the possibility to reduce the $E2$ transition matrix elements for a seniority conserving transition between configurations j^n to those in j^ν . This can be a great simplification since for the many nuclei the low-energy states have a low seniority.

Interacting Boson Model

The Interacting Boson Model (IBM or IBA) [16] is an algebraical model based on group theory and used to describe the collective properties of the nuclei. The collective properties of the nucleus depend only on valence nucleons and they form pairs called s - and d -bosons of angular momenta $l = 0$ and $l = 2$ respectively. The s and d bosons have between them six magnetic substates and the system can be viewed as a six dimensional space. This six dimensional system can be mathematically described in terms of the algebraic structure of the six-dimension unitary group $U(6)$. Each of the three subgroups corresponds to a geometrical limit [17, 18, 19, 20, 21].

This version of the IBA model does not distinguish between the valence protons and neutrons. This version is known in the literature as the IBA-1 model. An extension of this model that takes into account the degrees of freedom of the protons and those of the neutrons is the IBA-2 model. Another extension of the IBA model, known as the Interacting Boson-Fermion Model (IBFM), couples a valence fermion to an even-even core and it is used to describe odd-A nuclei.

Nucleon-Pair Approximation

The Nucleon-Pair Approximation model uses a phenomenological shell model Hamiltonian and calculates the matrix elements in a pair basis of identical nucleons coupled to spin-zero [22]. This provides an efficient truncation of the shell model by shrinking the dimension of the model space which makes possible to due calculations for the medium and heavy nuclei.

Large Scale Shell-Model calculations

The Large Scale Shell-Model (LSSM) calculations are a combination of shell-model calculations and different algorithms or truncations. The LSSM calculations can use large valence spaces which allows them to include the most important degrees of freedom. These algorithms include the Monte Carlo shell model [23, 24] or the Monte Carlo diagonalization method [25]. These type of calculations are probably the best solution for future of the theoretical nuclear structure models.

Gamma spectroscopy possibilities at the ROSPHERE multi-detector array

ROSPHERE multi-detector array

ROSPHERE is a multi-detector γ -ray spectrometer mounted on the first experimental line of the 9 MV Tandem accelerator of IFIN-HH, near Bucharest, Romania [26]. The array is constructed to accommodate up to 25 detectors in a spherical geometry, Compton suppressed HPGe detectors, $\text{LaBr}_3(\text{Ce})$ scintillators and neutron scintillation detectors.

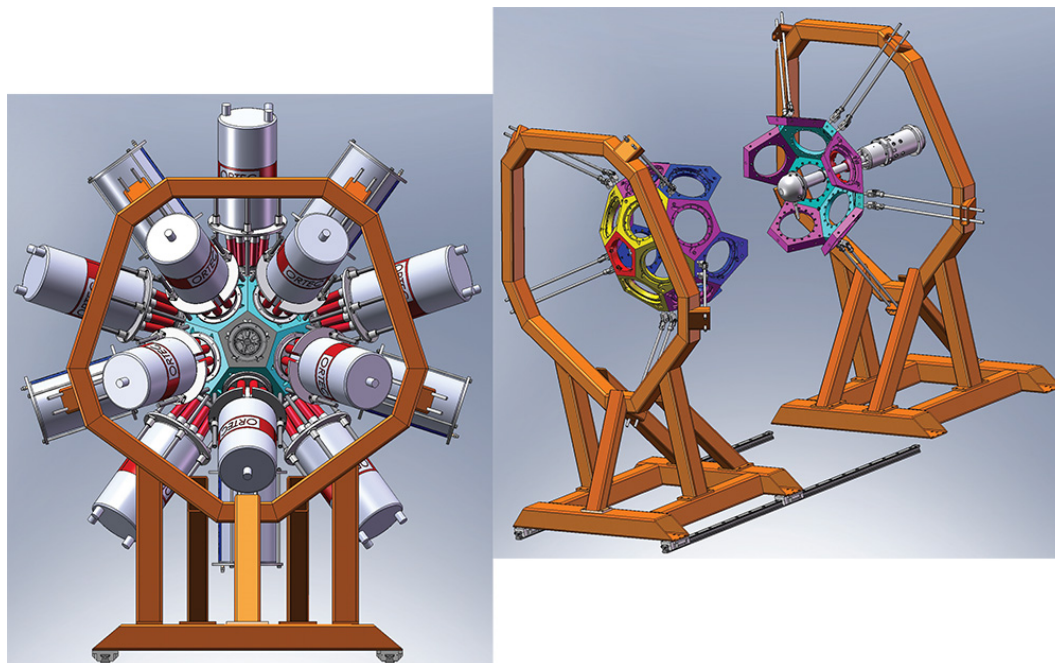


Figure 3.1: A CAD representation of ROSPHERE spectrometer. On the left is a representation of the spectrometer viewed along the beam axis, and on the right one can distinguish the five angular rings of the array and a plunger device.

ROSPHERE is designed and built for lifetime measurements of excited nuclear states over a wide range of times, typically from tens of femtoseconds to the tens of nanoseconds range. The lifetime of an excited nuclear state represents an experimental observable sensitive to the underlying structure of that nuclear state. Through the reduced matrix elements, the lifetimes provide information on the wavefunctions of the states involved in the transition.

The array is usually run in a mixed configuration comprised of 15 Compton suppressed HPGe detectors and 10 LaBr₃(Ce) scintillators. In this configuration one can measure nuclear lifetimes using DSAM and in-beam FEST methods, or, by using the Bucharest plunger device [27], RDDS and in-beam FEST methods. In this way one can measure over a longer time domain.

Typical measurements

Fusion-evaporation reactions

One of the most convenient way of producing high spin excited states with a large cross section is through fusion-evaporation reactions. The desired nuclear states are populated through the compound nucleus reaction mechanism, first described by Niels Bohr [28]. The reaction is typically represented as:



Due to the large angular momentum that is transferred to the compound nucleus, the fusion-evaporation reactions populate high-spin states, making them ideal to study nuclear structure at high spin and high multiplicity. Another useful characteristic of fusion-evaporation reactions is the production of nuclei with oriented states, as consequence of the reaction kinematics [29, 30].

Nuclear decay

Another way of populating the excited levels is through β decay. The main advantage of the β decay population of the excited nuclear states is the clean experimental γ spectra. The production of excited nuclei through beta decay by using a fusion-evaporation reaction can be represented as:



The B^* reaction product is created in an excited state by means of nuclear reactions. This then decays through beta decay populating excited nuclear states in the nucleus of interest C .

Heavy-ion sub-barrier transfer reactions

The transfer reaction at energies near and below the Coulomb barrier are governed by the distance of the closest approach between the projectile and the target [31, 32]. The reaction will take place if the distance is short enough for the nuclear forces to come into play. This minimum distance is for small values of the impact parameter b .

Due of the low impact factor, only a small angular momentum is transferred to the recoil and, as consequence, only low spin states are populated. Because of this, heavy-ion sub-barrier transfer reactions have low multiplicity. This characteristic can be used to separate the experimental spectra of γ -rays emitted by nuclear states populated through the higher multiplicity reactions such as fusion-evaporation reactions.

Experimental techniques

Recoil Distance Doppler Shift method

The Recoil Distance Doppler Shift (RDDS) method is an experimental technique used to measure lifetimes of excited nuclear states in the 10^{-12} to 10^{-8} s range [33]. The nuclei of interest are produced through nuclear reaction in a thin enough target to allow the recoil to eject from the target. The nucleus flies in vacuum until it is stopped in a thick foil, known as a stopper.

The energies of the γ -rays which decay the nuclear states of the in-flight nuclei are affected by the Doppler effect. This energy shift depends on the velocity v of the nucleus and on the angle θ with respect to the travelling direction at which the γ -ray is emitted:

$$E_s = E_0 \frac{\sqrt{1 - \beta^2}}{1 - \beta \cos \theta} \approx E_0 (1 + \beta \cos \theta) , \quad (3.3)$$

where E_s is the shifted energy and E_0 is the energy of the same transition emitted by the nucleus at rest.

The lifetimes are extracted from the dependence of the ratio between the intensities of the shifted and unshifted components with the distance between the target and the stopper. The ration from which one can extract the lifetime is:

$$R = \frac{I_0}{I_s + I_0} = \exp(-d/v\tau) . \quad (3.4)$$

Doppler Shift Attenuation method

In the Doppler Shift Attenuation method (DSAM) the lifetimes of the excited nuclear states are compared to the stopping time of the recoil in the target or in a backing. This method allows for the measurement of lifetimes in the 10^{-15} to 10^{-12} s range, comparable with the stopping time of the recoil in the target (backing).

The average energy of the γ -rays emitted in-flight is:

$$\bar{E}_s(\theta) \approx E_0 \left(1 + \frac{\bar{v}}{c} \cos \theta \right) , \quad (3.5)$$

where \bar{v} is the average velocity of the recoil. If the velocity of the recoil is small the lifetime can be extracted through the centroid method, as the centroid shifts with the angle of the emitted γ -ray, by determining \bar{v} and comparing it to a theoretically determined value. If the speed of the recoils is large enough, the Doppler effect will produce a characteristic γ lineshape. Based on the materials stopping power, the lifetime can be determined from the analysis of the lineshape of the transition of interest.

In-beam Fast Electronic Scintillation Timing method

The Fast Electronic Scintillation Timing (FEST) method is a direct way of measuring the decay curve via nuclear electronic modules. The time curve is constructed by measuring the

time difference between the population and the decay of the nuclear state, usually with two fast scintillation detectors, *e.g.* LaBr₃(Ce) or BaF₂.

The time difference between the feeding transition and the decaying transition is measured with a time to amplitude converter (TAC) or with a time to digital converter (TDC). The logic START and STOP signals are given by the constant fraction discriminators (CFDs) from the signal coming from the detectors.

A method suitable for in-beam γ -ray spectroscopy using triple γ coincidences has been developed by our group [2, 26]. This method is presented in Chapter 5.

Angular Correlation measurements

The directional distribution of radiation from an ensemble of oriented nuclei is given by [27, 34]:

$$W(\theta) = \sum_k A_k P_k(\cos \theta), \quad (3.6)$$

where θ is the angle between the direction of emission and the orientation axis, A_k is the angular distribution coefficient and $P_k(\cos \theta)$ are the Legendre polynomials. Usually only the $k = 0, 2, 4$ give significant contributions and typical experiment yields a distribution of the following form [35]:

$$W(\theta) = A_0 P_0(\cos \theta) + A_2 P_2(\cos \theta) + A_4 P_4(\cos \theta). \quad (3.7)$$

The values of A_0 , A_2 and A_4 can be obtained by fitting the distribution to Eq. 3.7 and the multipolarity of the transition determined.

Another way of measuring the polarity of a transition is by selecting certain substates by measuring in coincidence with another transition. This method is used in the case of nuclear decay when the nuclear states are not oriented. The anisotropy of angular distribution will depend on the angle between the two transitions and on the multipolarity of the transitions. To determine the multipolarity of the transition of interest one needs to know the polarity of the coincident transition.

DCO ratios method

Directional Correlations of γ -rays de-exciting Oriented states measurements are used to determine transition multipolarities and spins, based on the angular correlation of successive emitted γ -rays which decay oriented nuclear states. The angular position of the detectors is noted with φ , the angle between the two planes and the beam axis. The position of the detectors about the beam axis is given by the θ_1 and θ_2 angles.

The DCO ration is [36]:

$$R_{DCO} = \frac{W(\theta_2, \theta_1, \varphi)}{W(\theta_1, \theta_2, \varphi)}. \quad (3.8)$$

The $W(\theta_2, \theta_1, \varphi)$ term is the intensity of the transition γ_2 in detector 2 determined in coincidence with the transition γ_1 in detector 1. The $W(\theta_1, \theta_2, \varphi)$ term is the intensity of the transition γ_2 in detector 1 determined in coincidence with the transition γ_1 in detector 2.

Lifetime measurements of excited nuclear states using the Recoil Distance Doppler Shift method and ROSPHERE

The Recoil Distance Doppler Shift (RDDS) method compares the lifetime of the excited nuclear states with the time of flight of the recoil. It is based on the Doppler effect which affects the emitted gammas while the recoil is in-flight.

In the singles RDDS analysis a high number of levels have to be taken into account and the way of extracting the lifetimes of nuclear state i is by solving differential equations of the following type:

$$\frac{d}{dt} n_i(t) = -\lambda_i n_i(t) + \sum_j^N \lambda_j n_j(t) b_{ji}, \quad (4.1)$$

where $n_i(t)$ and $n_j(t)$ are the number of nuclei found in levels i and j at the time t , the number of the highest feeding level is N and b_{ji} are the branching ratios of the levels j with respect to the level i . The decay constants λ_j of the levels j are the inverse of the states lifetimes τ_j as $\lambda_j = 1/\tau_j$.

For the singles analysis one has to know in advance the intensities of the γ transitions and the branching factor of the transition between the levels j and i . The transitions of the same energy cannot be analysed and taken correctly into account in the analysis of other states.

Bucharest plunger device

RDDS measurements require a device able to achieve and maintain a target to stopper distance in the low μm range. The distances must be maintained throughout the measurement with a high accuracy. Such a device is known in the literature as a plunger device.

The Bucharest plunger device is constructed based on the design of the coincidence plunger developed at Institute for Nuclear Physics (IKP) of the University of Cologne [37]. A schematic representation of the device is presented in Fig. 4.1.

The distance between the target and the stopper is monitored using the capacitance method. A step signal of constant amplitude is applied to the stopper with a frequency of 250 Hz. The

voltage induced on the target is read through a classical amplifier, an analogue to digital converter (ADC) and a multichannel analyser (MCA) to a computer.

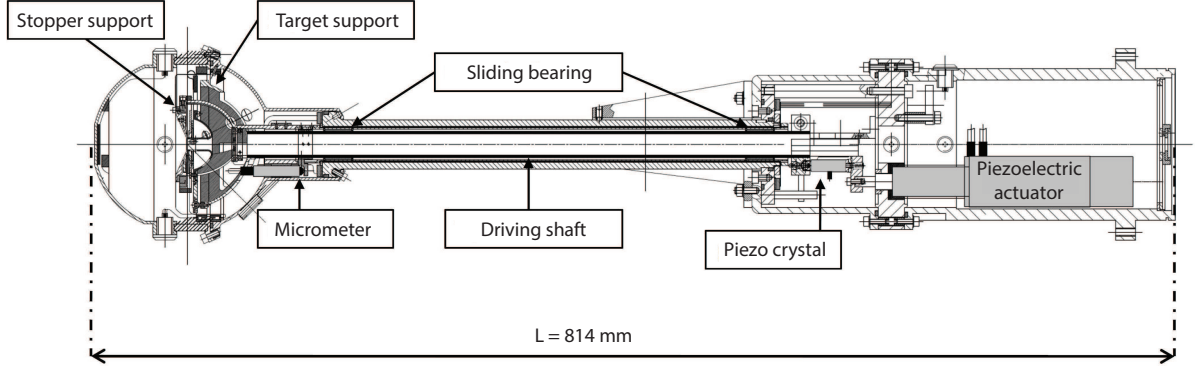


Figure 4.1: Schematic representation of the Bucharest plunger device. Figure taken from [27].

Differential Decay Curve method in $\gamma - \gamma$ coincidence

The DDCM analysis was developed to simplify the RDDS analysis and later was extended for all the lifetime measurement methods which use the Doppler effect [38, 39]. In DDCM analysis a lifetime can be determined for each target to stopper distance. For an unambiguous determination of the lifetime and three target-stopper distances are needed, measured in the sensitivity region [37]. The DDCM $\gamma - \gamma$ coincidence analysis further more simplifies the determination of the lifetimes.

Using the integral form of Eq. 4.1 one can arrive at the equation for the lifetime of state i in the DCCM analysis:

$$\tau_i = \frac{-N_i(t) + \sum_j^N N_j(t) b_{ji}}{\frac{d}{dt} N_i(t)}. \quad (4.2)$$

In the DDCM $\gamma - \gamma$ coincidence analysis the most used types of conditioning are the direct and the indirect ones. For the former, a gate on the shifted component of the transition which directly feeds the level of interest is used. For the latter one, a gate on the shifted component of the transition which indirectly feeds the level of interest through an intermediary level is used.

In the direct conditioning Eq. 4.2 becomes [38]:

$$\tau_i = \frac{I_{u_A}^{sB}(x)}{\frac{d}{dx} I_{s_A}^{sB}(x)} \frac{1}{v}. \quad (4.3)$$

The intensities $I_{u_A}^{sB}(x)$ are experimentally measured for each target to stopper distance. The time derivative which fits the Doppler shifted intensities $I_{s_A}^{sB}(x)$ is estimated by region fitting the $I_{u_A}^{sB}(x)$ using second degree polynomials which are continuous and differentiable.

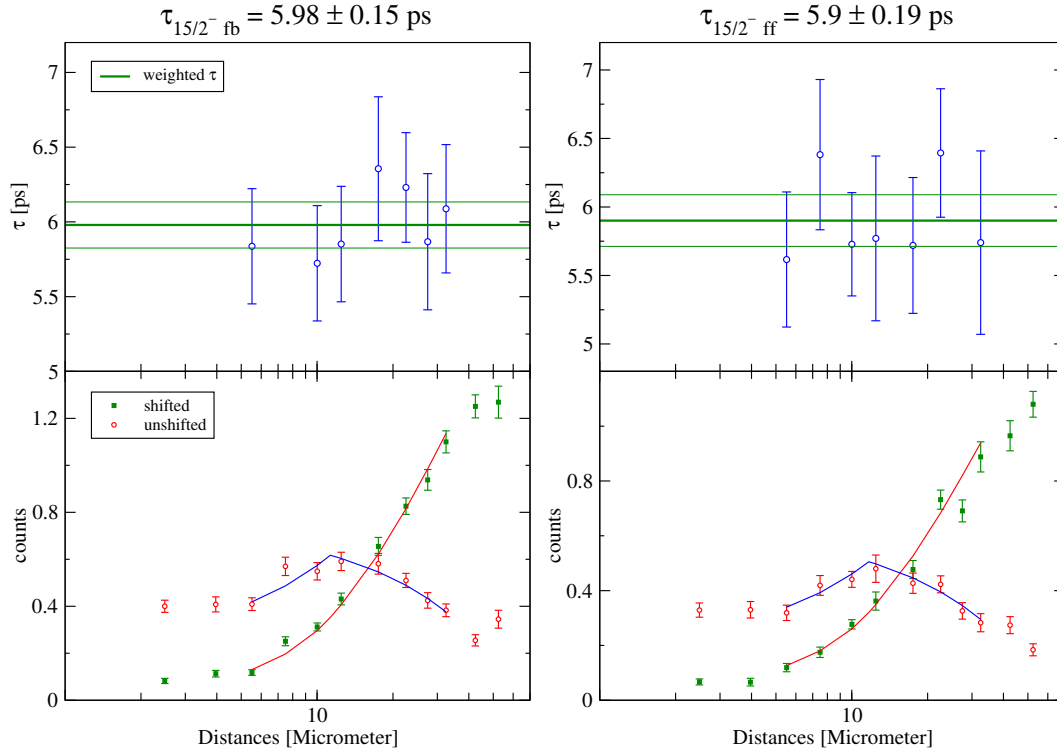


Figure 4.2: Results of the DDCM analysis for the $15/2^-$ state. In the left panel is the analysis for the “bw” ring and in the right panel the one for the “fw” ring. Figure taken from [26].

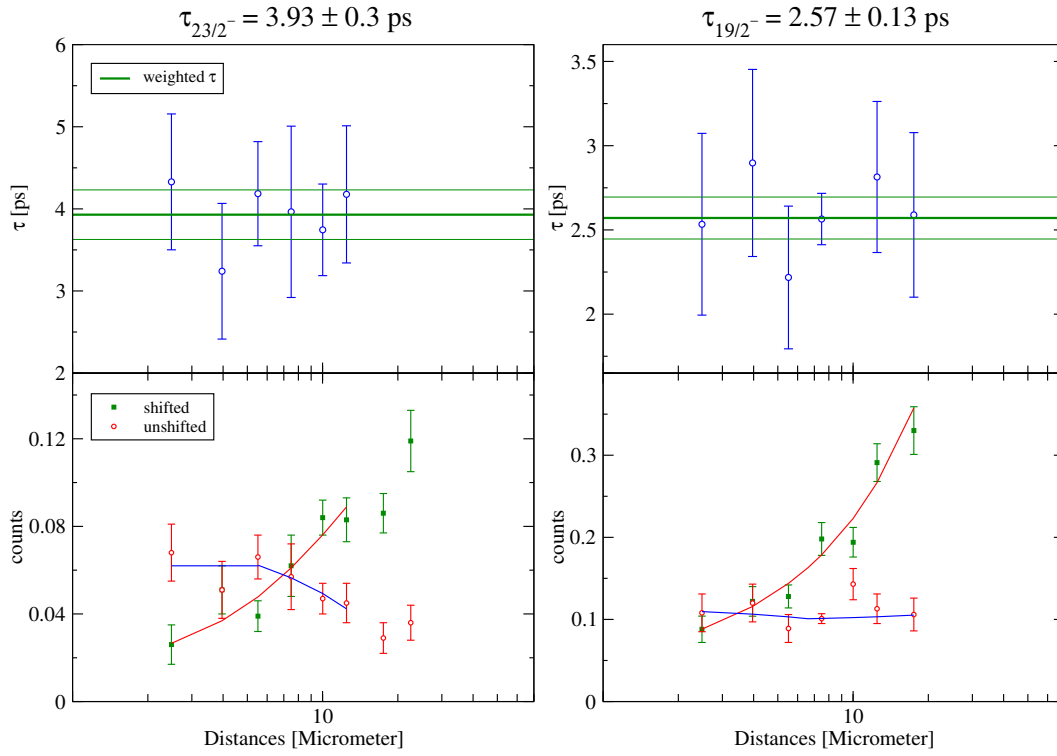


Figure 4.3: DDCM analysis for the $23/2^-$ state (left hand panels) and $19/2^-$ state (right hand panels) in ^{119}Te . Figure taken from [26].

In the case of indirect conditioning the Eq. 4.2 becomes [38]:

$$\tau_i = \frac{I_{u_A}^{sC}(x) - \alpha I_{u_B}^{sC}(x)}{\frac{d}{dx} I_{u_A}^{sC}(x)} \frac{1}{v}, \quad (4.4)$$

where x is the target to stopper distance, v is the velocity of the recoil nucleus and:

$$\alpha = \frac{I_{u_A}^{sC}(x) + I_{s_A}^{sC}(x)}{I_{u_B}^{sC}(x) + I_{s_B}^{sC}(x)}. \quad (4.5)$$

Lifetimes measurements in ^{119}Te

The excited states in ^{119}Te were populated in the $^{110}\text{Pd}(^{13}\text{C}, 4n)$ reaction using a 2 pnA ^{13}C beam with an energy of 50 MeV that bombarded a 0.7 mg/cm² self supported ^{110}Pd target. A 4 mg/cm² gold stopper was used to stop the recoils. The beam was provided by the Bucharest 9 MV Tandem accelerator at IFIN-HH.

The emitted γ rays were detected using the ROSPHERE multi-detector array. The experimental setup consisted of 14 HPGe detectors and 11 LaBr₃(Ce) scintillation detectors. Data was measured for 15 target-to-stopper distances, from 7 to 83 μm , using the trigger condition of two HPGe detectors in coincidence OR three detectors in coincidence, one HPGe AND two LaBr₃(Ce).

DDCM analysis of the 640-keV transition which de-excited the $15/2^-$ state was performed for both “fw” and “bw” spectra which were obtained by gating on the shifted component of 718-keV transition detected at 37° in the “fw” ring. In the bottom panels of Fig. 4.2, the squares represent the normalised intensities of the shifted component $I_{s_A}^{sB}(d)$ and the circles represent unshifted component $I_{u_A}^{sB}(d)$. The curves represent the fits of each term of Eq. 4.3. In top panels are the τ values calculated for each distance and the resulting mean lifetime.

Table 4.1: Calculated $B(E2)$ values in this analysis for transitions de-exciting the first yrast states in ^{119}Te .

E_{niv} (keV)	E_γ (keV)	$J_i^\pi \rightarrow J_f^\pi$	τ (ps)	$B(E2)$ (W.u.)
901.26	640.3	$15/2^- \rightarrow 11/2^-$	5.9(4)	36.8(27)
1618.96	717.7	$19/2^- \rightarrow 15/2^-$	2.6(3)	47.4(53)
2272.46	653.5	$23/2^- \rightarrow 19/2^-$	3.9(5)	37.6(49)

A similar DDCM analysis was performed for the $19/2^-$ state. To extract the lifetime of the $19/2^-$ state, I put a gate on the shifted component of the 653-keV transition that feeds the state and I analysed the 718-keV transition detected in coincidence with it. The analysis was performed for both “fw” and “bw” rings. To extract the lifetime of the $23/2^-$ state, I put a gate on the shifted component of the 1075-keV transition that feeds the state and I analysed the 653-keV transition detected in coincidence with it.

Nuclear lifetime measurements using the in-beam fast-timing technique at ROSPHERE

The Fast Electronic Scintillation Timing (FEST) technique is an evolution of the Delayed Coincidence methods [40, 41, 42] made possible by then new BaF₂ fast scintillation detectors which have a very good time resolution of $\sim 100 - 300$ ps, when paired with a thin β detector, and an energy resolution of $\sim 10\%$ at $E_\gamma = 0.6$ MeV [42, 43].

In the $\beta\gamma\gamma$ coincidence fast-timing measurements the lifetime is extracted from the $\beta\gamma$ time-delayed coincidence between a thin plastic scintillator which detects the β -particles and a crystal scintillator which detects the γ -rays. The scintillation detectors are coupled to fast photomultiplier tubes (PMTs) to ensure the best timing resolution.

The time difference between the population and the decay of a nuclear state is electronically measured and from this difference the decay curve is constructed. The fast-timing method represents a direct way of measuring the nuclear lifetimes using electronic methods.

In-beam fast-timing

In time, a scintillation crystal better suited for fast-timing has been developed. This is the LaBr₃(Ce) crystal which has a time resolution of $100 - 300$ ps (depending on the crystal size) and an energy resolution of $2 - 3\%$ at 662 keV, due to the high light output and fast decay time [26]. Using the LaBr₃(Ce) detectors a new technique was developed at IFIN-HH [2]. The technique is developed for lifetime measurements using in-beam γ -ray spectroscopy of fusion-evaporation or of fragmentation reactions.

A schematic representation of the technique is presented in Fig. 5.1. An array containing both HPGe and LaBr₃(Ce) detectors are measuring in triple-gamma coincidence the emitted γ -rays. The high energy resolution of HPGe detectors allows the selection of cascade of interest, while the LaBr₃(Ce) detectors are used to build the time spectra for the level of interest.

One can set a gate in the HPGe detectors on the full energy peak of the γ_1 transition to enhance the transitions above and to be able to select them in the LaBr₃(Ce) detectors. With this gate on the HPGe detectors one constructs an $E_\gamma E_\gamma \Delta T$ three-dimensional coincidence matrix, with the energy detected in one LaBr₃(Ce) detector on the x -axis and the energy detected in the

other LaBr₃(Ce) detector on the y -axis. On the z -axis, the time difference between the detection of the two γ -rays is stored.

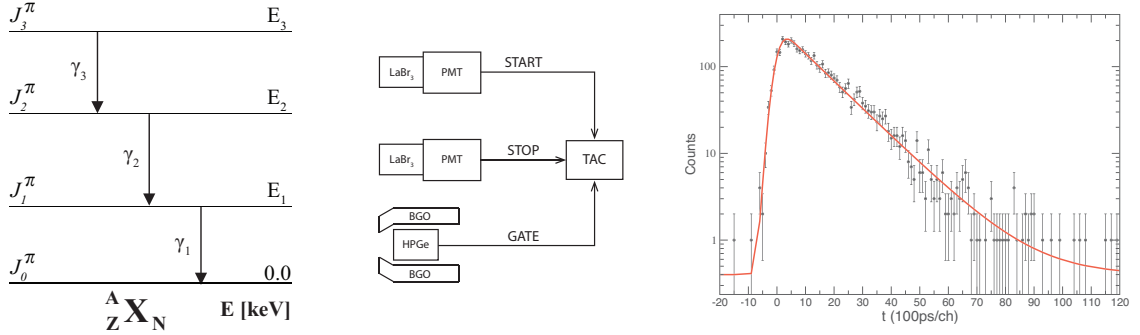


Figure 5.1: Schematic representation of the in-beam fast-timing technique.

The in-beam fast-timing technique is best suited for the axial symmetric spectrometers, *e.g.* the ROPHERE spectrometer [26], where one can take advantage of their high efficiency. In order to use all the possible combinations between the LaBr₃(Ce) detectors of such a spectrometer, one has to correct the time walk of each individual detector and to align the detectors time wise.

Constant Fraction Discriminator

The constant fraction discriminator (CFD) is the electronic device which gives a logic signal representing the time reference of each signal coming from the detectors. In a CFD, a bipolar signal is created from the input signal coming from the detectors and, by detecting the zero crossing of the bipolar signal, the logic signal is created. To create the bipolar signal, the input signal is delayed using an internal delay which can be extended using an external delay. Then, a fraction from the undelayed signal is subtracted from the input signal.

The slope of the bipolar pulse is dependent on the input amplitude. This is the case for both of the CFD timing modes. The charge sensitivity of the zero crossover comparator is dependant on the slope of the bipolar signal. This in turn translates in dependence on the input amplitude. Another source of timing uncertainty is represented by the noise added on top of the input signal and the noise generated by the CFD itself.

Walk correction

The walk correction performed for the data presented in the present work is done using full energy peaks of a ¹⁵²Eu source, a well known and studied radiation source that is available in all laboratories. The full energy peak walk correction eliminates the shift that may be caused by the average lifetime of the transitions that make up the the Compton background [43]. This improves the attainable precision of walk correction.

The walk correction needs to be validated. This is usually accomplished by remeasuring one or more known lifetimes of nuclear states which were populated in the same experiment as the states of interest for which the analysis is to be performed.

Lifetime extraction methods from the delayed time spectra

Centroid shift method. This method is usually used when the lifetime τ to be measured is much shorter than the FWHM of the prompt response function. In the ideal case when there are no feeding and no background contributions, as per definition the centroid (“center of gravity” [44]) of the delayed time distribution is shifted by the lifetime from the centroid $M^{(1)}[f(t)]$ position of its corresponding $PRF(t)$.

Deconvolution method. The method is used if the length of lifetime τ is comparable to the FWHM of the prompt response function. The delayed time distribution is the convolution of a Gaussian distribution, *i.e.* the PRF, and an exponential [45].

Slope method. In the slope method, one does not use the time distribution of the prompt spectrum. The method is used when the lifetime τ to be measured is longer than the FWHM of the prompt response function. The value of the lifetime is not affected by the prompt contribution of other cascades if it is much longer than the FWHM of the prompt response function.

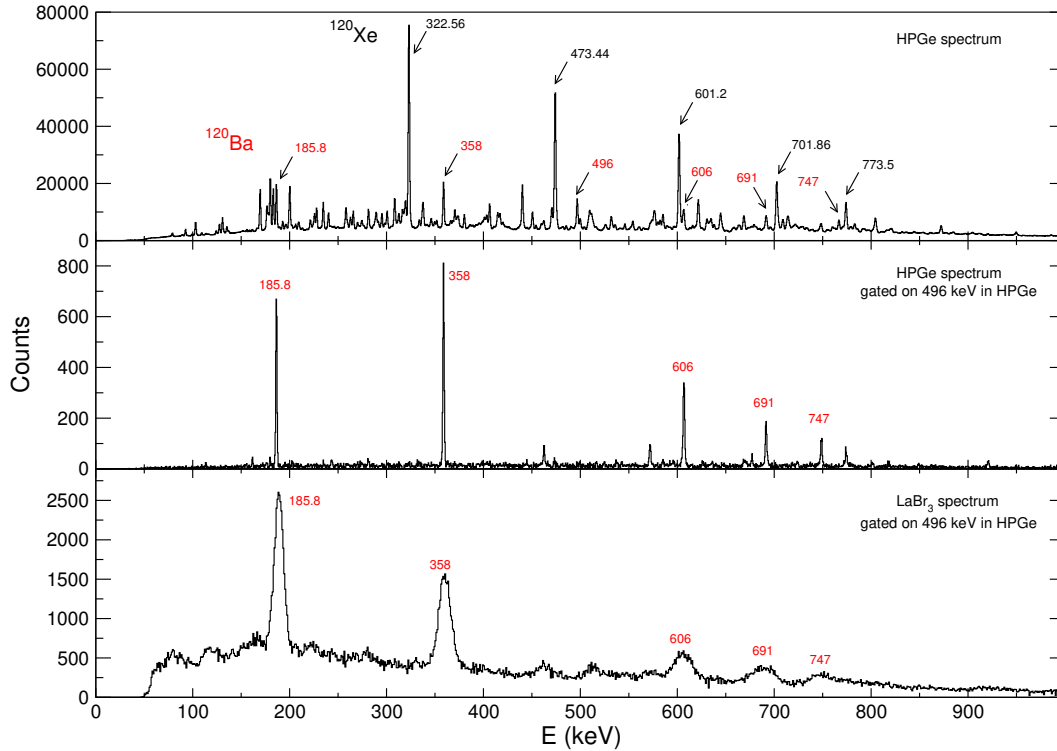


Figure 5.2: Measured experimental spectra for the $^{106}\text{Cd}(^{16}\text{O},2n)^{120}\text{Ba}$ reaction.

Lifetime of the first 2^+ state in ^{120}Ba

The excited states in ^{120}Ba were populated via the $^{106}\text{Cd}(^{16}\text{O},2n)^{120}\text{Ba}$ fusion-evaporation reaction. The $\sim 5 \text{ mg/cm}^2$ self-supported target was bombarded by a beam of ^{16}O with an intensity of $\sim 2 - 3 \text{ pA}$ at an energy of 64 MeV. The beam was provided by the Bucharest 9 MV Tandem accelerator at IFIN-HH and the γ -rays were measured with the ROSPHERE spectrometer.

The experimental setup consisted of 14 HPGe detectors and 11 LaBr₃(Ce) scintillation detectors. The experimental data were taken in about three days using the trigger condition of two HPGe detectors in coincidence OR three detectors coincidence, one HPGe AND two LaBr₃(Ce) detectors. The walk correction was performed using a ~ 250 kBq ^{152}Eu source. The time energy dependence was corrected using the method described in Section 5 and was validated using the lifetime of the first 4^+ state in ^{152}Sm .

I sorted the measured data in two $E_\gamma E_\gamma \Delta T$ three-dimensional coincidence matrices using for each one a gate in the HPGe detectors, one on the 496-keV transition and one on the associated background. The matrices were cut using two bi-dimensional conditions on the energy, one on the coincidence between the 358-keV transition which feeds the 2^+ state and the 185.8-keV transition that decays it and the other one was on the associated background. The background timing spectrum was subtracted from the full energy peak coincidence spectrum, first for the LaBr₃(Ce) coincidences and then for the HPGe gates.

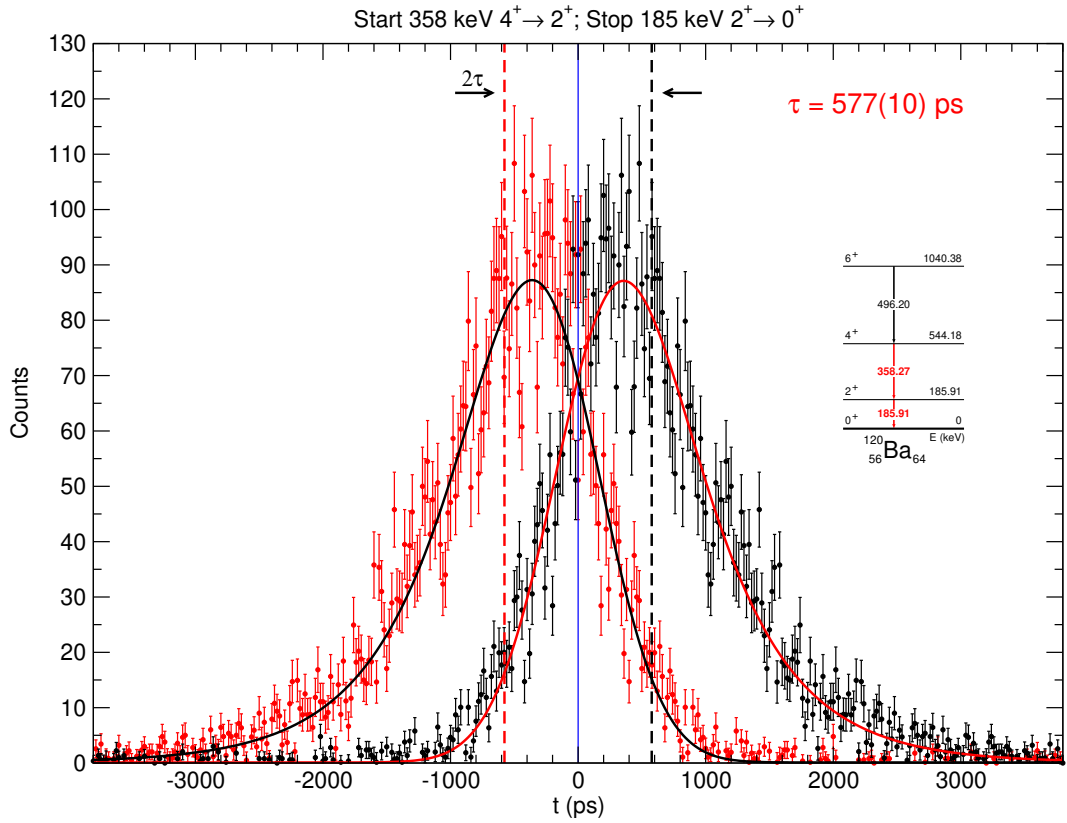


Figure 5.3: The delayed and the anti-delayed time spectra obtained for the first 2^+ state in ^{120}Ba .

The obtained delayed spectrum is presented in Fig. 5.3 with black full circles. The red line represents the convolution of the prompt response function and the lifetime of the 2^+ state. The anti-delayed time spectrum was obtained by inverting the exciting and the de-exciting transitions in the analysis. The difference between the centroids of the two distributions is equal to twice the lifetime of the state, which I measured to be $\tau = 577(10)$ ps. The uncertainty of the result reflects only the statistical uncertainty. Using the lifetime, I calculated the value of the reduced transition probability that connects the 2^+ state to the ground state to be $B(E2; 2^+ \rightarrow 0^+_{gs}) = 149(3)$ W.u.

Precision fast-timing measurements in neutron-deficient Po isotopes at IFIN-HH

At the time of writing this paper, there are only a small number of known lifetimes of the low lying yrast states of the Po isotopes around $A = 210$. The measured lifetimes of the 2_1^+ states are in the ps range and they were determined through Coulomb excitation. The 8_1^+ states are long lived isomers and their lifetimes were measured using electronic timing methods. The lifetimes of the 4^+ and 6^+ are difficult to measure due to the long time difference between the lifetime of the 8^+ state and the lifetime of the 2^+ state.

To measure the lifetime of the low lying yrast states in the neutron deficient Polonium isotopes I used the fast in-beam timing method. In order to extract the lifetimes of the 2^+ states the lower range of the method was extended by performing precise walk corrections.

Walk correction

A necessary and key step in the fast-timing analysis is the correction of the time walk. The accuracy of the correction will limit the range of measurable lifetimes and the precision with which they can be determined. This is even more significant when measuring lifetimes that are close to the lower limit of the fast-timing method, in the low ps range.

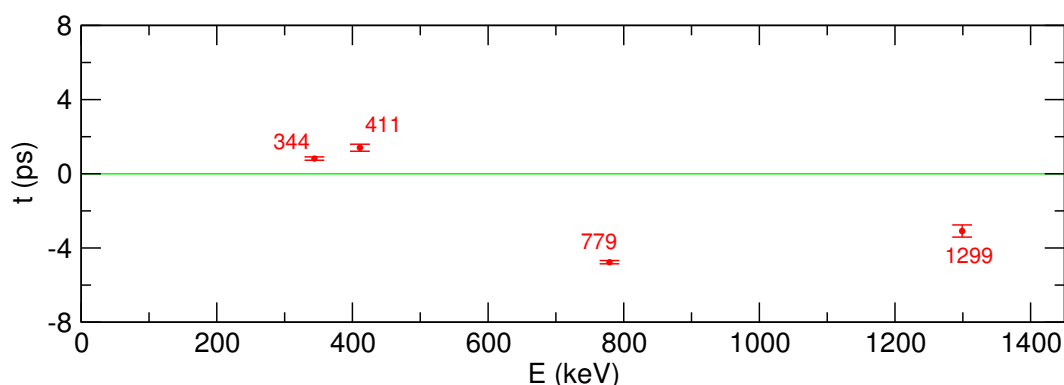


Figure 6.1: The time-walk curve for the combined $\text{LaBr}_3(\text{Ce})$ detectors in the ROSPHERE array.

The walk correction was performed using a ~ 45 kBq ^{152}Eu laboratory radiation source. The time-energy dependence was corrected using the method described in Section 5. To evaluate and

validate the result of the walk correction, the lifetimes of the first 2^+ state in $^{202,204}\text{Pb}$ were determined and compared with the experimental data and the predictions available in the literature. The value obtained for the lifetime of the 2_1^+ state in ^{204}Pb is $\tau = 3.5 \left(\begin{smallmatrix} +57 \\ -35 \end{smallmatrix} \right)$ ps. and the value obtained for the lifetime of the 2_1^+ state in ^{202}Pb is $\tau = 3.2 \left(\begin{smallmatrix} +47 \\ -32 \end{smallmatrix} \right)$ ps.

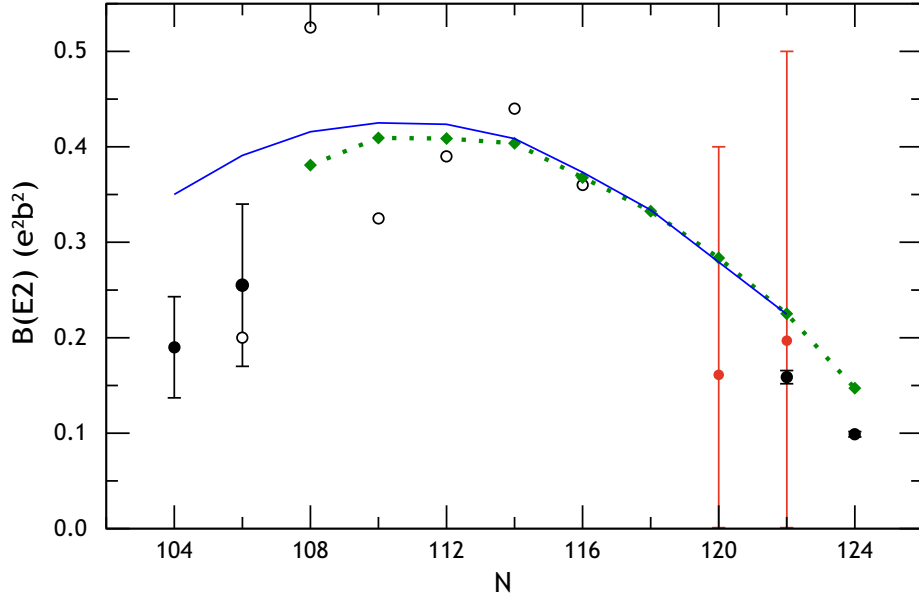


Figure 6.2: Systematics values of the $B(E2; 2_1^+ \rightarrow 0_{gs}^+)$ in Pb isotopes [46] and the results obtained in the present analysis (red circles).

I compared the calculated values of the $B(E2; 2_1^+ \rightarrow 0_{gs}^+)$ in $^{202,204}\text{Pb}$ to the systematics in Pb isotopes [46]. A very good agreement between $B(E2)$ values from the measured lifetimes in $^{202,204}\text{Po}$ and the systematics. The good agreement and the large energy difference between the transitions used to measure the lifetimes of 2_1^+ states in $^{202,204}\text{Po}$ validate the walk correction.

Lifetime measurements in ^{202}Po

The excited states in ^{202}Po were populated in the $^{194}\text{Pt}(^{12}\text{C},4n)$ reaction. A ~ 1.1 pA ^{12}C beam with an energy of 62 MeV was impinged on a ~ 9.4 mg/cm 2 self supported ^{194}Pt target. The beam was provided by the Bucharest 9 MV Tandem accelerator at IFIN-HH. The γ rays were detected using the ROSPHERE multi-detector array. The experimental setup consisted of 14 HPGe detectors and 11 LaBr $_3$ (Ce) scintillation detectors. Data was taken for 12 days, using the trigger condition of two HPGe detectors in coincidence OR three detectors in coincidence, one HPGe AND two LaBr $_3$ (Ce).

Two approaches to separate the transitions in ^{202}Po from the other reaction channels were used in this analysis. In the first approach I selected the transitions in ^{202}Po using and isomer tagging in the HPGe detectors. The timing of the HPGe detectors was aligned to the timing of the fast LaBr $_3$ (Ce) detectors. Gates on the anticipated transitions above the isomer in the HPGe detectors allowed the selection of the transitions below the isomer in the LaBr $_3$ (Ce) detectors.

In the second approach, I used a multiplicity filter to limit the possible number of coincidences when constructing the $E_\gamma E_\gamma \Delta T$ three-dimensional coincidence matrices. The maximum number of selected coincidences was three. On top of this condition, I used gates in the HPGe detectors to select the transitions in ^{202}Po .

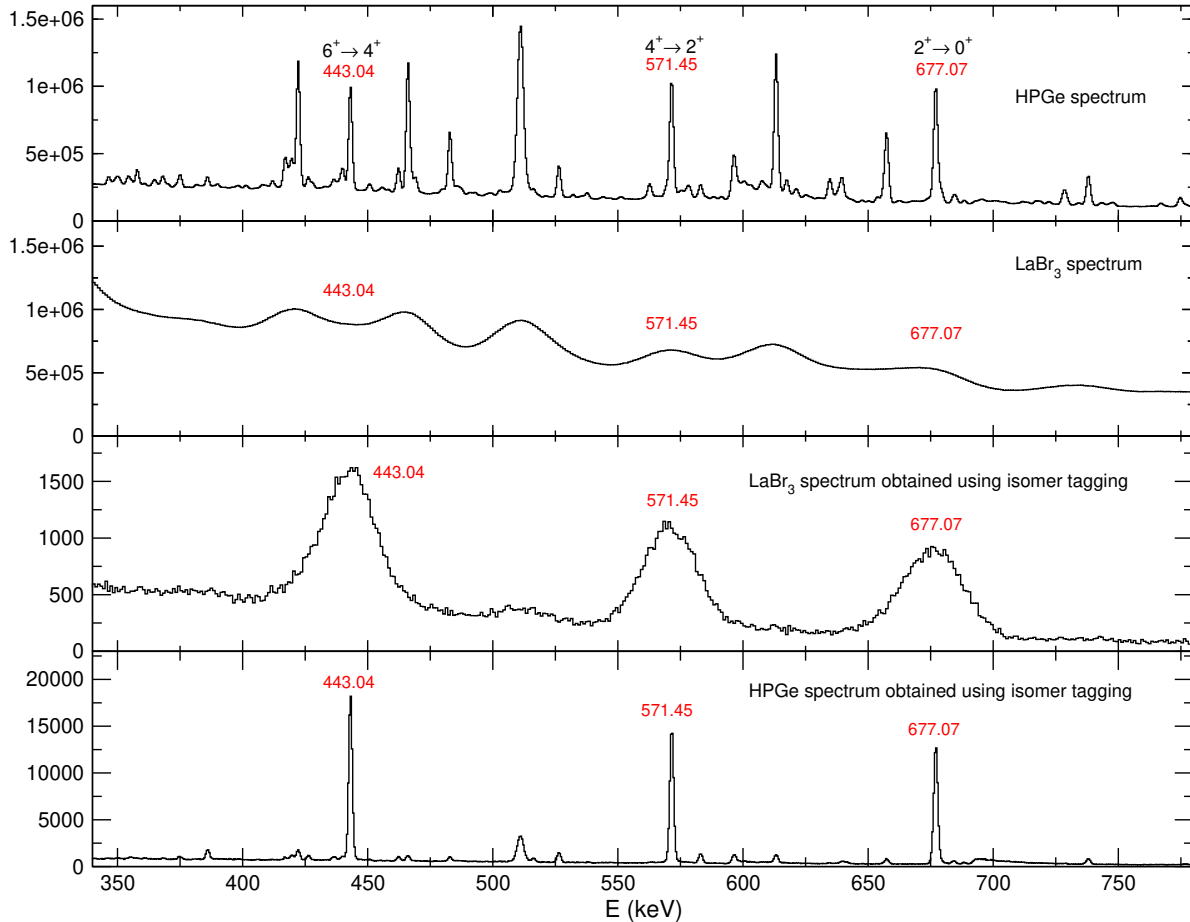


Figure 6.3: Measured experimental spectra for the $^{194}\text{Cd}(^{12}\text{C},4n)^{202}\text{Po}$ reaction.

The values were extracted using the centroid shift method and the obtained results were consistent between the two approaches. The value I obtained in this analysis for the lifetime of the 2_1^+ state is $\tau = 3.7(37)$ ps and for the lifetime of the 4_1^+ state is $\tau = 11.5(30)$ ps. The uncertainties of the lifetimes take into account the statistical uncertainty and accounts for the time-walk difference between the start and the stop energies.

The result I obtained for the lifetime of the 2_1^+ state in ^{202}Po , $\tau = 11.5(30)$ ps, is significantly longer than the value of $\tau = 2.53 \left(\begin{smallmatrix} +76 \\ -48 \end{smallmatrix} \right)$ ps previously measured in a Coulomb excitation experiment [7]. The only way I could verify the lifetimes determined in the presented analysis was by measuring the sum of the lifetimes of the 2_1^+ and of the 4_1^+ states in ^{202}Po . From the two approaches, only the isomer tagging allows for such an analysis.

The sum of the of the lifetimes of the 2_1^+ and of the 4_1^+ states was found to be shorter than the lifetime measured for the 2_1^+ state, but longer than that of the 4_1^+ state. The adopted value

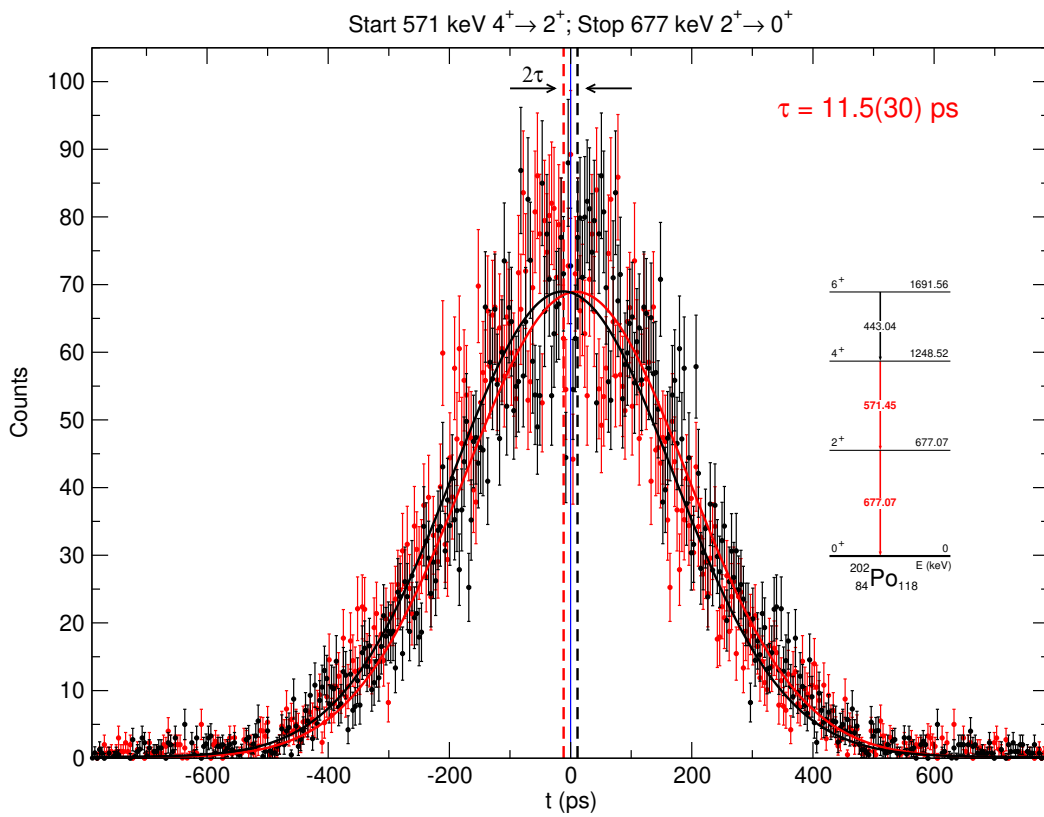


Figure 6.4: The delayed and anti-delayed time spectra for the 2_1^+ state in ^{202}Po .

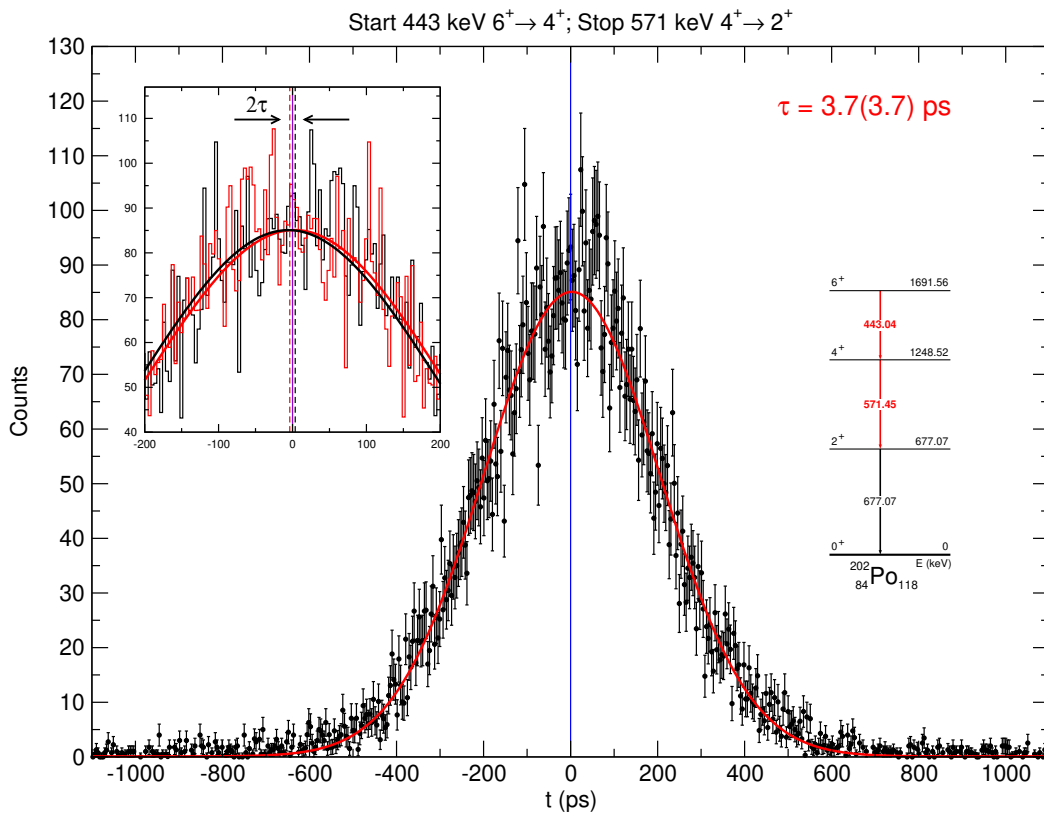


Figure 6.5: Time delayed spectrum which corresponds to the lifetime of the 4_1^+ state in ^{202}Po .

for the lifetimes of the two states is less than the obtained sum of the two, $\tau_{2_1^+, 4_1^+} < 8$ ps. With the values of the lifetime, I calculated the value of the reduced transition probabilities $B(E2; 4_1^+ \rightarrow 2_1^+) > 24$ W.u. and $B(E2; 2_1^+ \rightarrow 0_{gs}^+) > 10$ W.u.

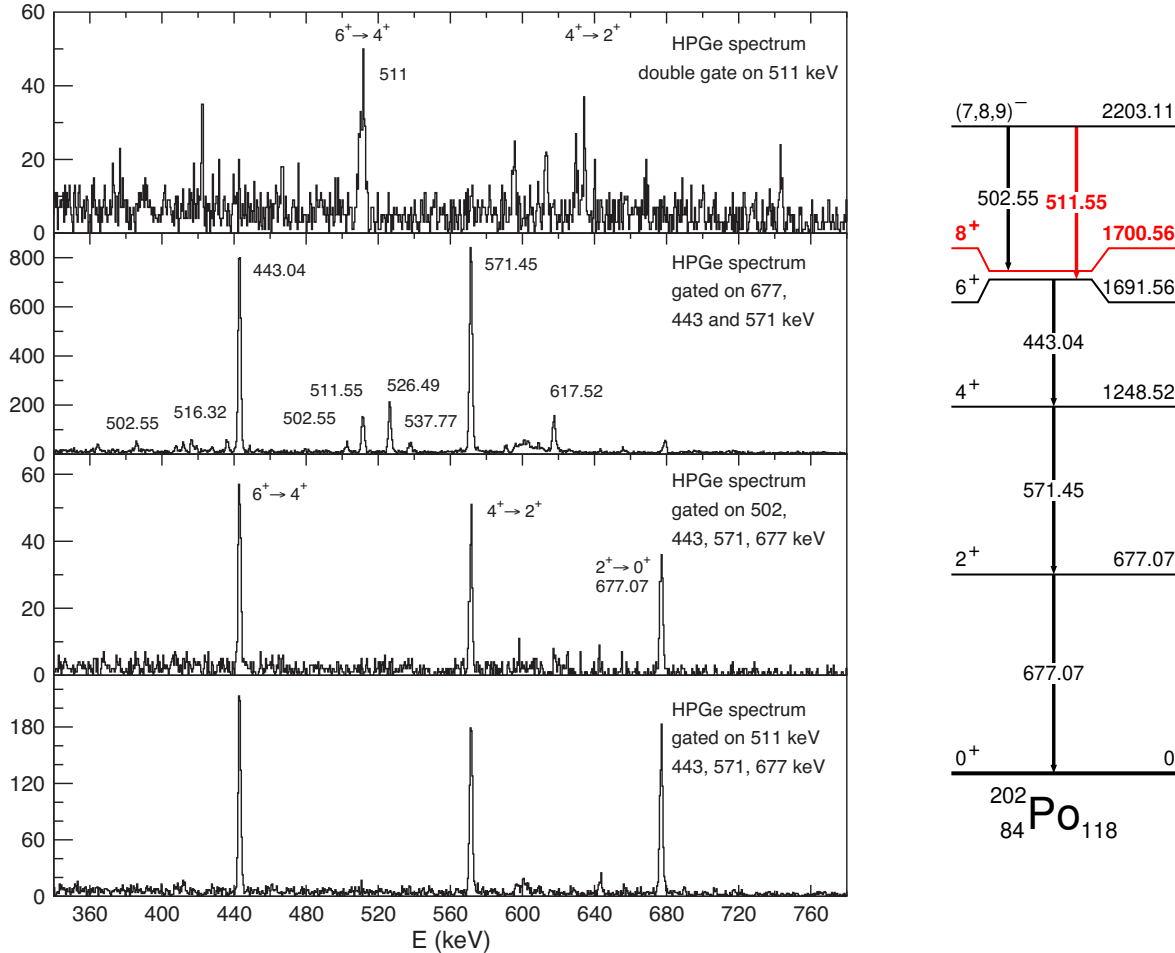


Figure 6.6: Spectra used to determine the energy of the $8_1^+ \rightarrow 6_1^+$ transition.

Before this analysis, the lifetime of the 8_1^+ state in ^{202}Po was known, but the energy of the $8_1^+ \rightarrow 6_1^+$ transition was unknown. This made impossible the calculation of the reduced transition probability $B(E2)$ which connects the two states.

Table 6.1: Calculated $B(E2)$ values for transitions de-exciting the first yrast states in ^{202}Po .

E_{niv} (keV)	E_γ (keV)	$J_i^\pi \rightarrow J_f^\pi$	τ (ps)	$B(E2)$ (W.u.)
677.07	677.07	$2_1^+ \rightarrow 0_{gs}^+$	< 8	> 10
1248.52	571.45	$4_1^+ \rightarrow 2_1^+$	< 8	> 24
1700.56	(9)	$8_1^+ \rightarrow 6_1^+$	$15.87(22) \cdot 10^4$	5.4(9)

The energy of the $8_1^+ \rightarrow 6_1^+$ transition was determined to be 9 keV and using the known lifetime of the 8_1^+ state, I calculated the value of $B(E2; 8_1^+ \rightarrow 6_1^+) = 5.4(9)$ W.u.

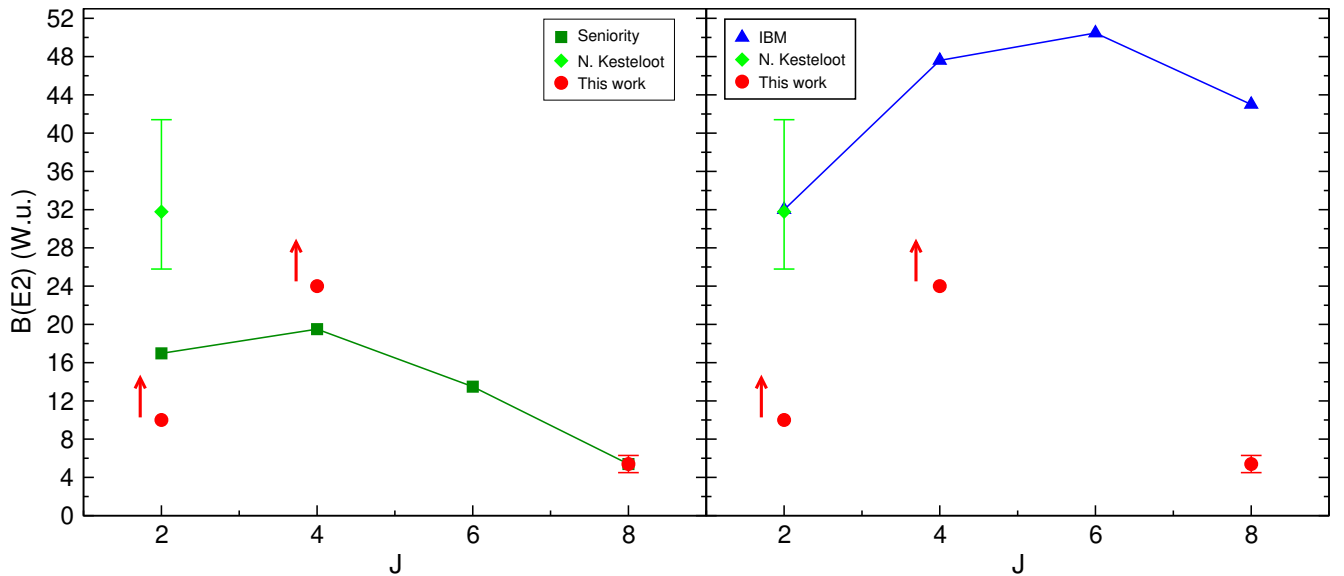


Figure 6.7: Comparison of the experimental values with the theoretical predictions for ^{202}Po .

The results obtained in this analysis for the ^{202}Po are summarised in Table 6.1. I compared the values obtained in the present analysis with the calculated $B(E2)$ values calculated for a pure j^2 configuration using the single-particle matrix element $\langle j || T(E2) || j \rangle$ with [47]:

$$B(E2; J_i \rightarrow J_i - 2) = 4(2J_i - 3) \left\{ \begin{matrix} j & J_i - 2 & j \\ J_i & j & 2 \end{matrix} \right\}^2 |\langle j || T(E2) || j \rangle|^2. \quad (6.1)$$

This comparison is presented in the left panel of Fig. 6.7. In the right panel the results are compared with the theoretical predictions. It is difficult to assess the validity of the predictions since only limits were obtained for the values of the $B(E2)$ which connect the lowest yrast states in ^{202}Po .

Lifetime measurements in ^{204}Po

The excited states in ^{204}Po were populated in the $^{196}\text{Pt}(^{12}\text{C}, 4n)$ reaction. A ~ 1.5 pA ^{12}C beam with an energy of 62 MeV was impinged on a ~ 9.77 mg/cm 2 self supported ^{196}Pt target. The beam was provided by the Bucharest 9 MV Tandem accelerator at IFIN-HH. The γ rays were detected using the ROSPHERE multi-detector array. The experimental setup consisted of 14 HPGe detectors and 11 LaBr $_3$ (Ce) scintillation detectors. Data was taken for 7 days, using the trigger condition of two HPGe detectors in coincidence OR three detectors in coincidence, one HPGe AND two LaBr $_3$ (Ce).

As in the analysis for ^{202}Po , two approaches were used to separate the transitions in ^{204}Po from the transitions coming from the other reaction channels. In the isomer tagging analysis, gates are used in the HPGe on anticipated transitions above the isomer to select the transitions below the isomer in the LaBr $_3$ (Ce) detectors.

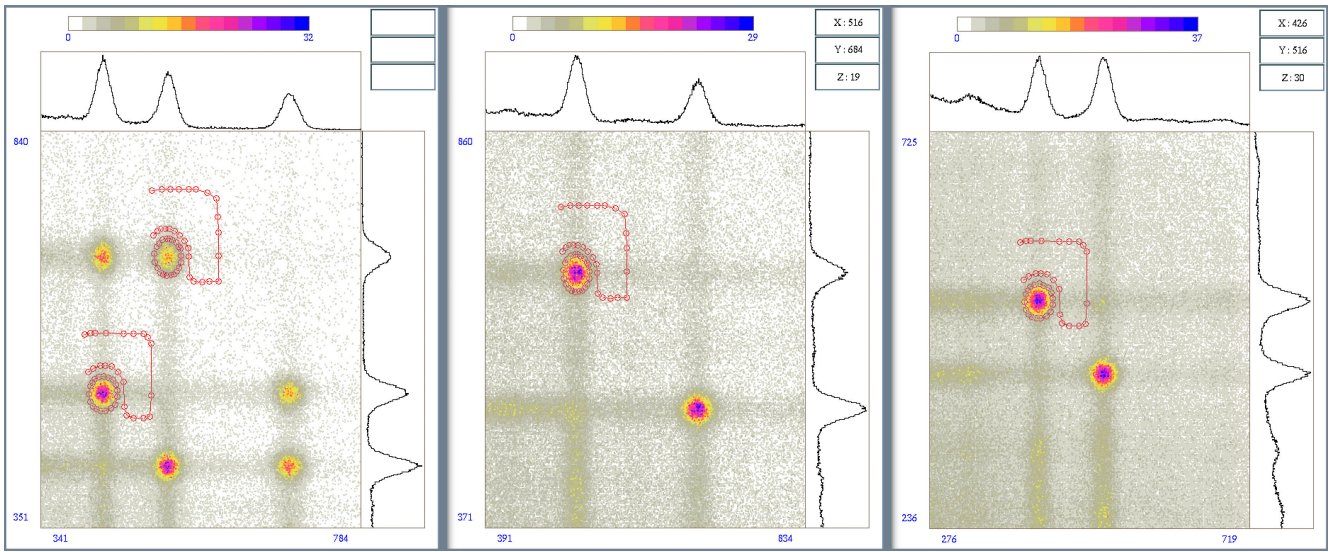


Figure 6.8: Energy projections with the bi-dimensional energy-energy conditions (*bananas*) used to extract the timing information from the $E_\gamma E_\gamma \Delta T$ coincidence matrix in the ^{204}Po analysis.

In the second approach, I used a multiplicity filter to limit to three the possible number of coincidences when constructing the $E_\gamma E_\gamma \Delta T$ three-dimensional coincidence matrices. I used gates in the HPGe detectors on the transitions that decay the 2_1^+ and 6_1^+ states and constructed four $E_\gamma E_\gamma \Delta T$ matrices.

In each of the two approaches I obtained values for the lifetimes for the 2_1^+ and of the 4_1^+ states. The values were extracted using the centroid shift method and the obtained results were consistent between the two approaches.

The value I obtained in this analysis for the lifetime of the 2_1^+ state in ^{204}Po is $\tau = 6.0(34)$ ps. The uncertainty of the lifetime takes into account the statistical uncertainty and accounts for the time-walk difference between the start and the stop energies. Using the lifetime, I calculated the value of the reduced transition probability that connects the 2_1^+ state to the ground state to be $B(E2; 2_1^+ \rightarrow 0_{gs}^+) = 12.5(70)$ W.u.

Table 6.2: Calculated $B(E2)$ values in the present analysis for transitions de-exciting the first yrast states in ^{204}Po .

E_{niv} (keV)	E_γ (keV)	$J_i^\pi \rightarrow J_f^\pi$	τ (ps)	$B(E2)$ (W.u.)
684.44	684.44	$2_1^+ \rightarrow 0_{gs}^+$	6.0(34)	12.5(70)
1200.95	516.51	$4_1^+ \rightarrow 2_1^+$	17.9(26)	16.9(25)

The value I obtained in this analysis for the lifetime of the 4_1^+ state in ^{204}Po is $\tau = 17.9(26)$ ps. The uncertainty of the lifetime takes into account the statistical uncertainty and accounts for the time-walk difference between the start and the stop energies. Using the lifetime, I calculated the value of the reduced transition probability that connects the 4_1^+ state to the 2_1^+ to be $B(E2; 4_1^+ \rightarrow 2_1^+) = 16.9(25)$ W.u.

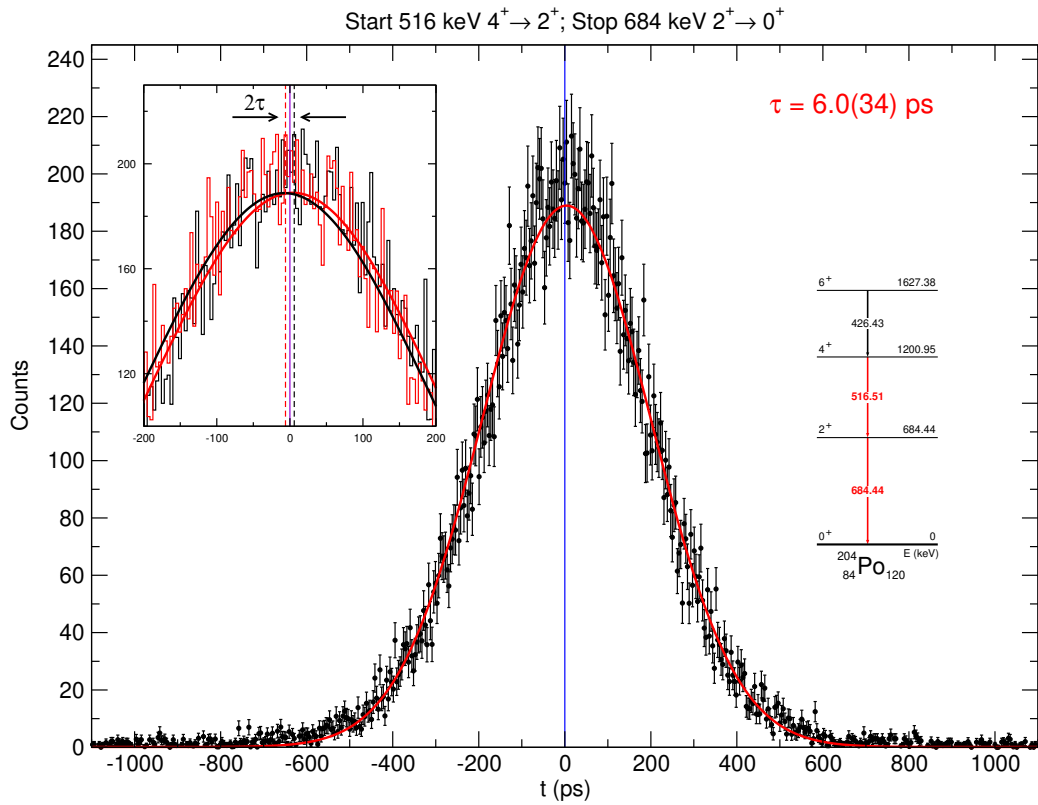


Figure 6.9: Time delayed spectrum which corresponds to the lifetime of the 2_1^+ state in ^{204}Po .

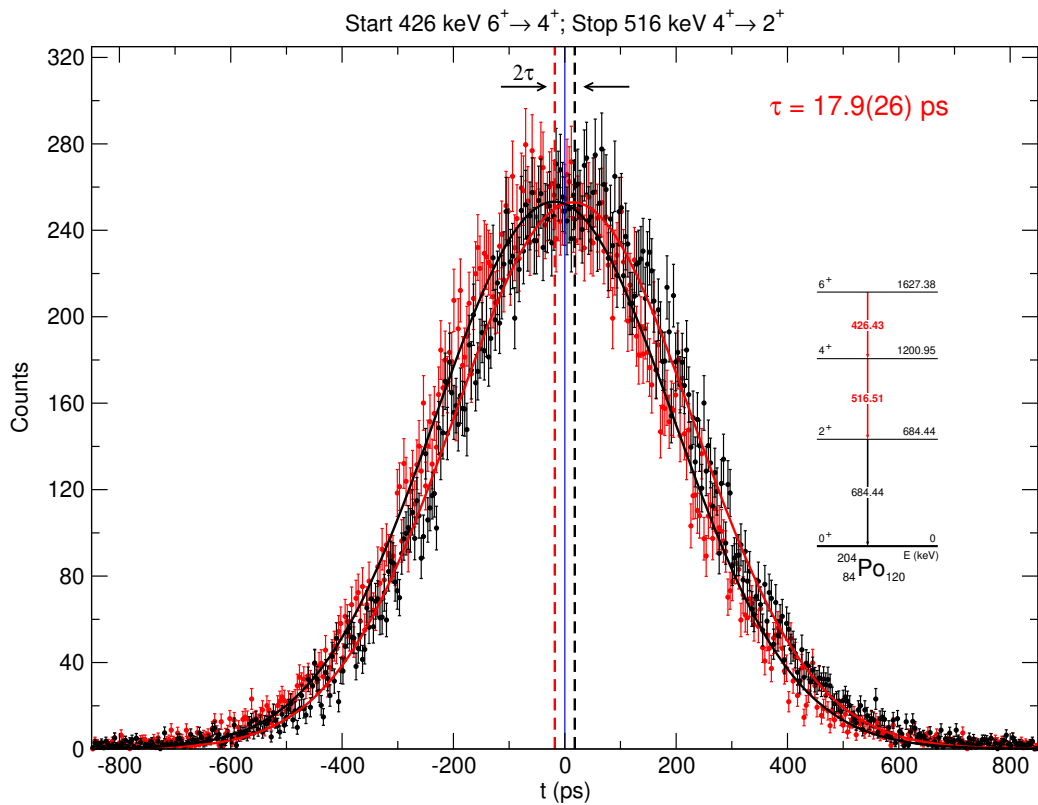


Figure 6.10: The delayed and anti-delayed time spectra for the 4_1^+ state in ^{204}Po .

The lifetimes determined in the presented analysis were verified by measuring the sum of the lifetimes of the 2_1^+ and of the 4_1^+ states in ^{204}Po in the matrix constructed in the isomer tagging analysis. The obtained sum is in agreement with the measured values.

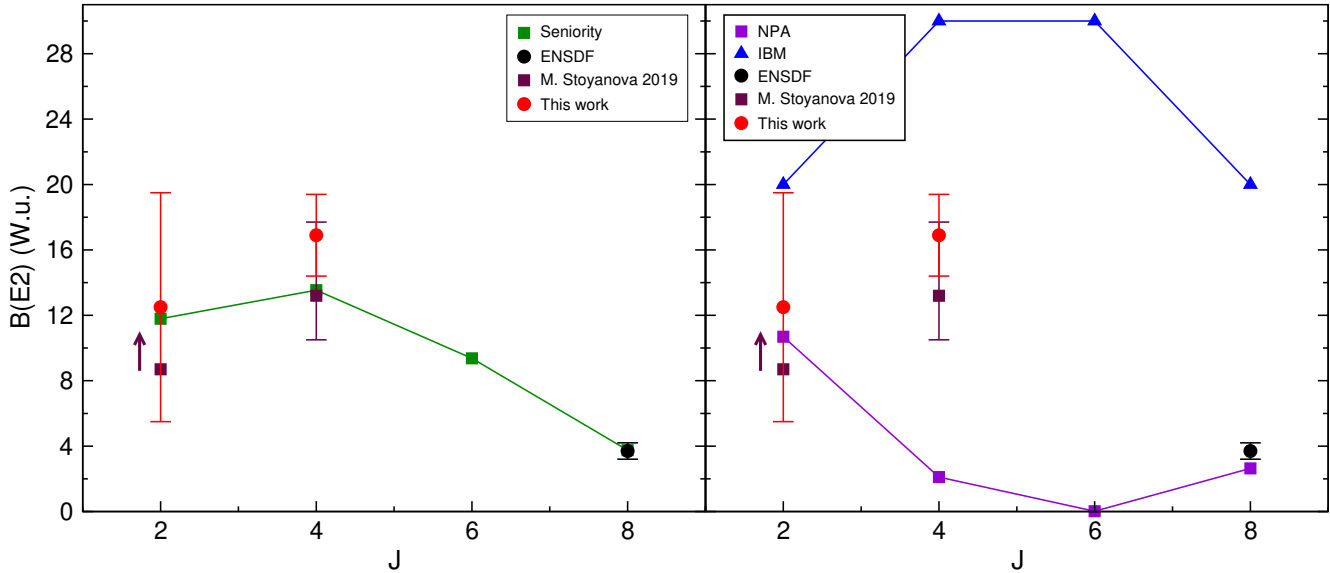


Figure 6.11: Comparison of the experimental values with the theoretical predictions for ^{204}Po .

The results obtained in this analysis for the ^{204}Po are summarised in Table 6.2. I compared the values obtained in the present analysis with the calculated $B(E2)$ values calculated for a pure j^2 configuration using Eq. 6. This comparison is presented in left panel of Fig. 6.11. In the right panel the results are compared with the available theoretical predictions. One can see that there is a good agreement with the predictions of the simple seniority calculations, but the predictions of the theoretical calculation [8, 9] are not in agreement with the experimental data.

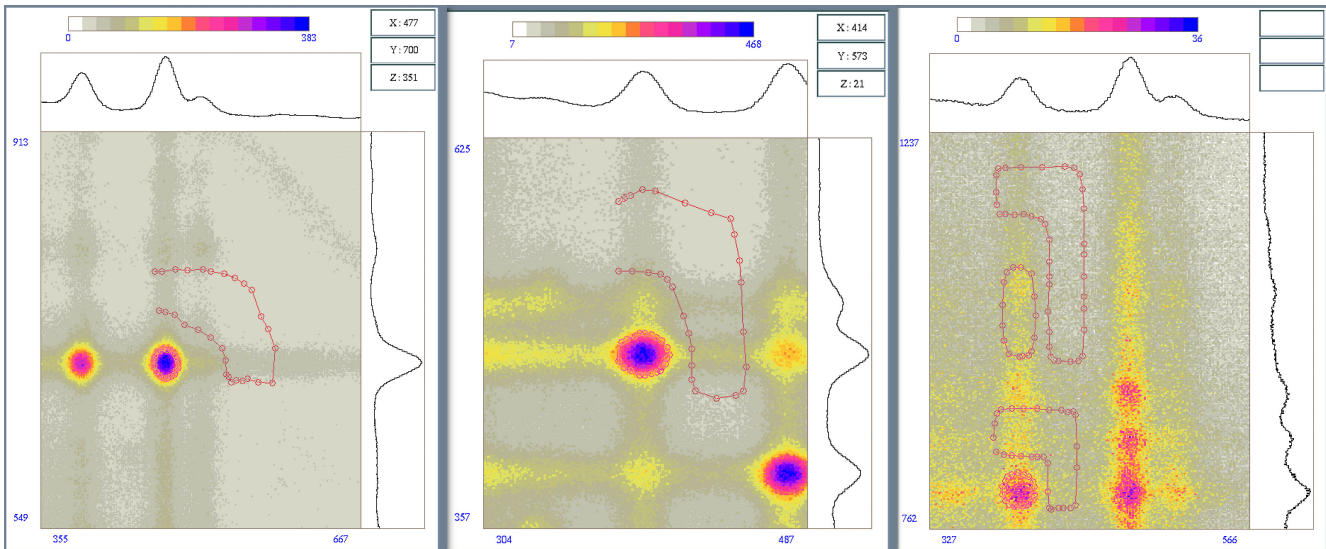


Figure 6.12: Energy projections with the bi-dimensional energy-energy conditions (*bananas*) used to extract the timing information from the $E_\gamma E_\gamma \Delta T$ coincidence matrix in the ^{206}Po analysis.

Lifetime measurements in ^{206}Po

The excited states in ^{206}Po were populated in the ϵ, β^+ decay of ^{206}At . The ^{206}At nuclei were populated in the $^{197}\text{Au}(^{13}\text{C}, 4n)$ reaction. A ~ 1.3 pA ^{13}C beam with an energy of 62 MeV was impinged on a ~ 9.78 mg/cm 2 self supported ^{197}Au target. The beam was provided by the Bucharest 9 MV Tandem accelerator at IFIN-HH. The γ -rays were detected using the ROSPHERE multi-detector array. The experimental setup consisted of 14 HPGe detectors and 11 LaBr $_3$ (Ce) scintillation detectors. Data was taken for 8 days, using the trigger condition of two HPGe detectors in coincidence OR three detectors in coincidence, one HPGe AND two LaBr $_3$ (Ce).

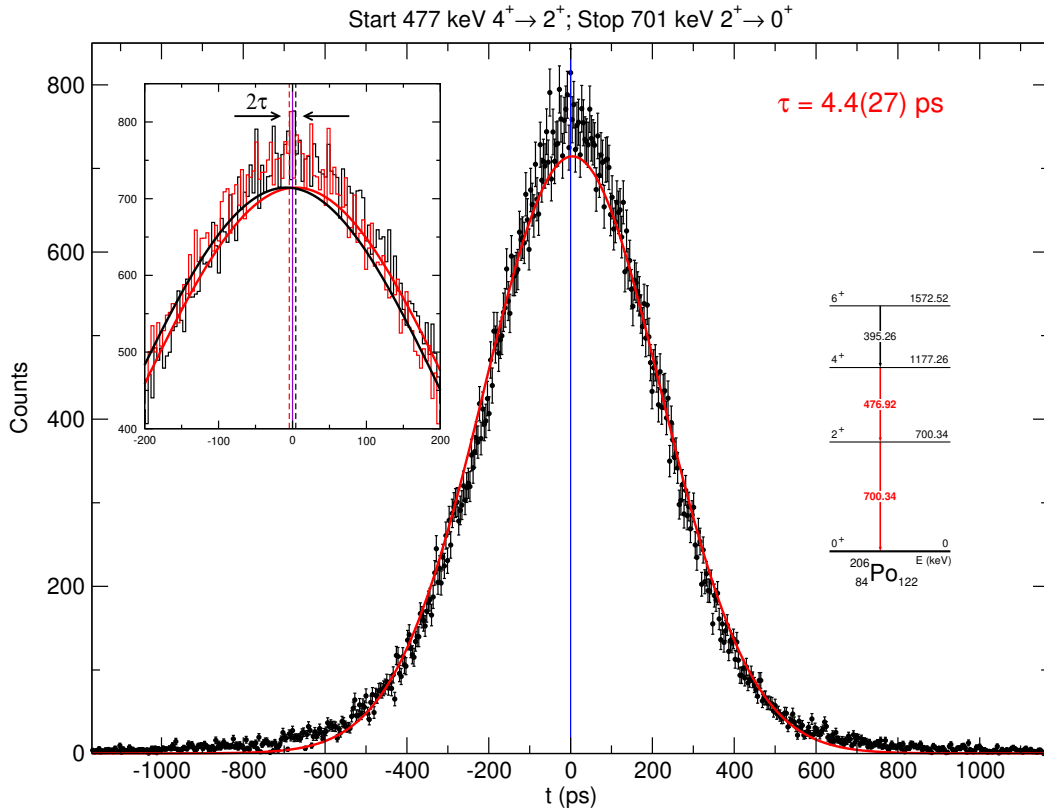


Figure 6.13: The delayed time spectra for the 2_1^+ state in ^{206}Po .

The beam bombarded the target to activate and accumulate ^{206}At . After the activation period, the beam was stopped, using a Faraday cup, and the decay was measured. ^{206}At has a half life $T_{1/2} = 30.6(8)$ min and the best activation-decay period combination was found to be half an hour intervals for each of them.

The value I obtained in this analysis for the lifetime of the 2_1^+ state in ^{206}Po is $\tau = 4.4(27)$ ps, value which was extracted using the centroid shift method. The uncertainty of the lifetime was estimated by independently measuring the lifetime in each of the LaBr $_3$ (Ce) used in the analysis. With the value of the lifetime, I calculated the value of the reduced transition probability $B(E2; 2_1^+ \rightarrow 0_{gs}^+) = 15.0(92)$ W.u.

The value I obtained in this analysis for the lifetime of the 4_1^+ state in ^{206}Po is $\tau = 79(2)$ ps.

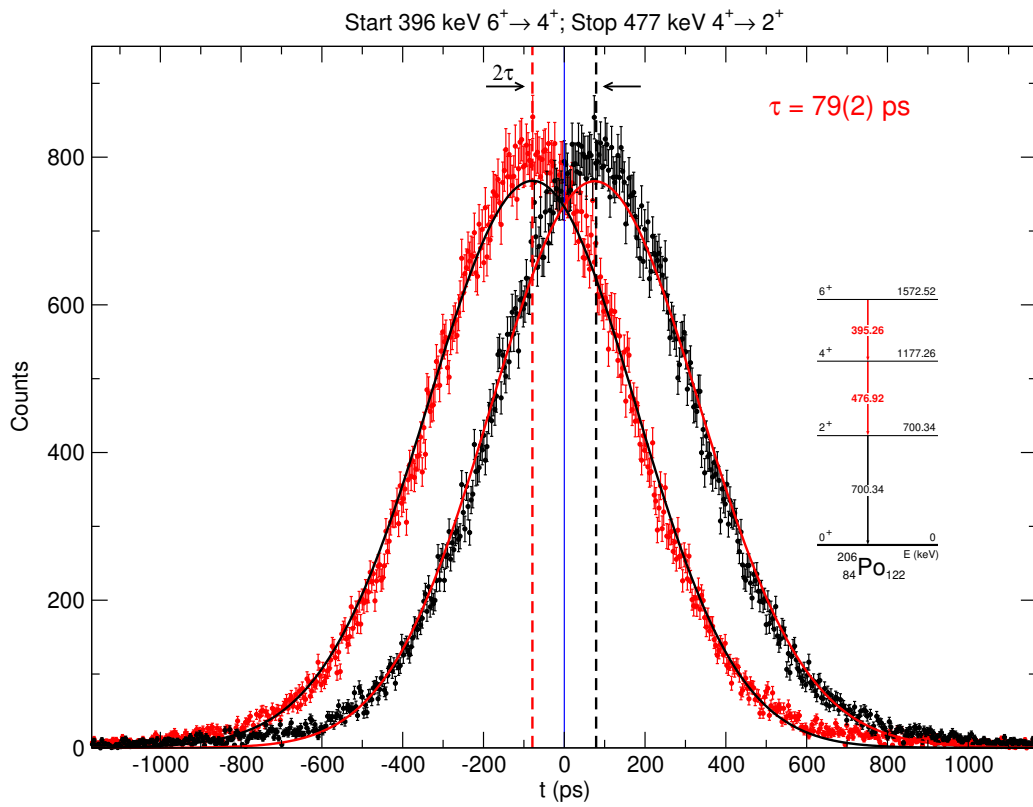


Figure 6.14: The delayed and anti-delayed time spectra for the 4_1^+ state in ^{206}Po .

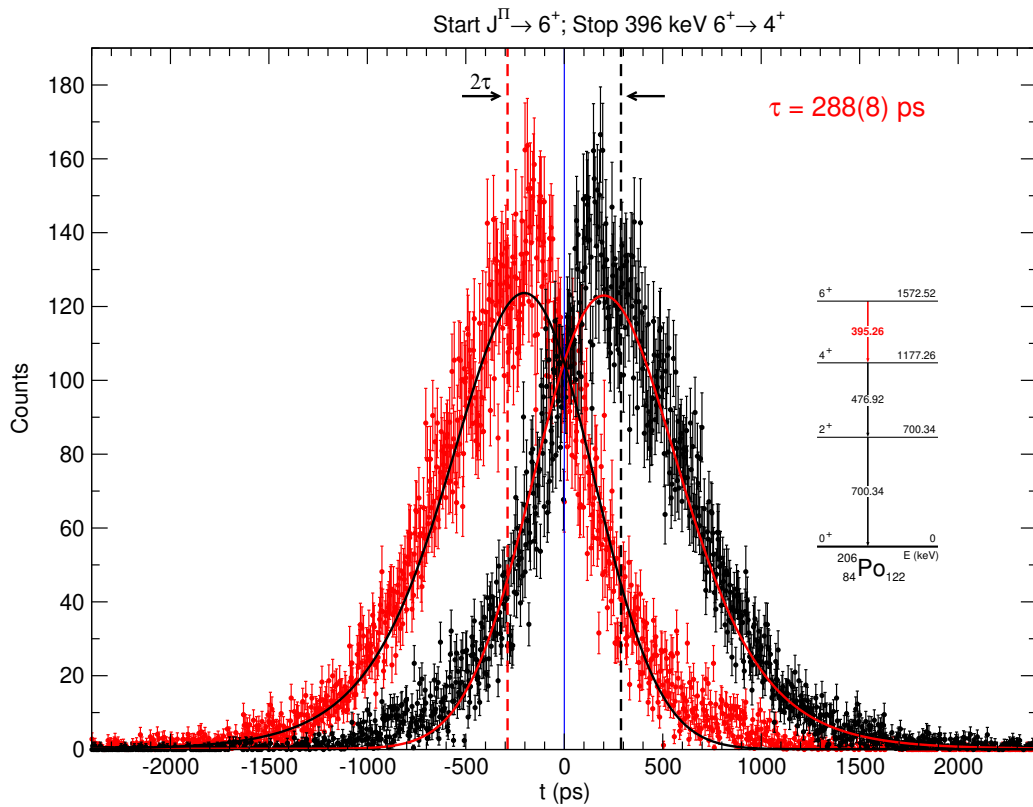


Figure 6.15: The delayed and anti-delayed time spectra for the 6_1^+ state in ^{206}Po .

The value of the lifetime was extracted using both the centroid shift method and the deconvolution method. The uncertainty of the lifetime takes into account the statistical uncertainty and accounts for the time-walk difference between the start and the stop energies. With the value of the lifetime, I calculated the value of the reduced transition probability $B(E2; 4_1^+ \rightarrow 2_1^+) = 5.60(11)$ W.u.

Table 6.3: Calculated $B(E2)$ values in the present analysis for transitions de-exciting the first yrast states in ^{206}Po .

E_{niv} (keV)	E_γ (keV)	$J_i^\pi \rightarrow J_f^\pi$	τ (ps)	$B(E2)$ (W.u.)
700.34	700.34	$2_1^+ \rightarrow 0_{gs}^+$	4.4(27)	15.0(92)
1177.26	476.92	$4_1^+ \rightarrow 2_1^+$	79(2)	5.60(11)
1572.52	395.26	$6_1^+ \rightarrow 4_1^+$	288(8)	3.84(11)

To extract the delayed timing spectra for the 6_1^+ state, I used four bi-dimensional conditions on the coincidence between two energy regions where I found transitions which primarily feed the 6_1^+ state and the 395.26-keV transition which de-excites the state and two on the associated background. Among these transitions are transitions that feed the isomer state. The contribution of the transitions which feed the 8_1^+ to the lifetime of the 6_1^+ was evaluated and was found to have no influence due to the large time difference between the lifetimes of the two states.

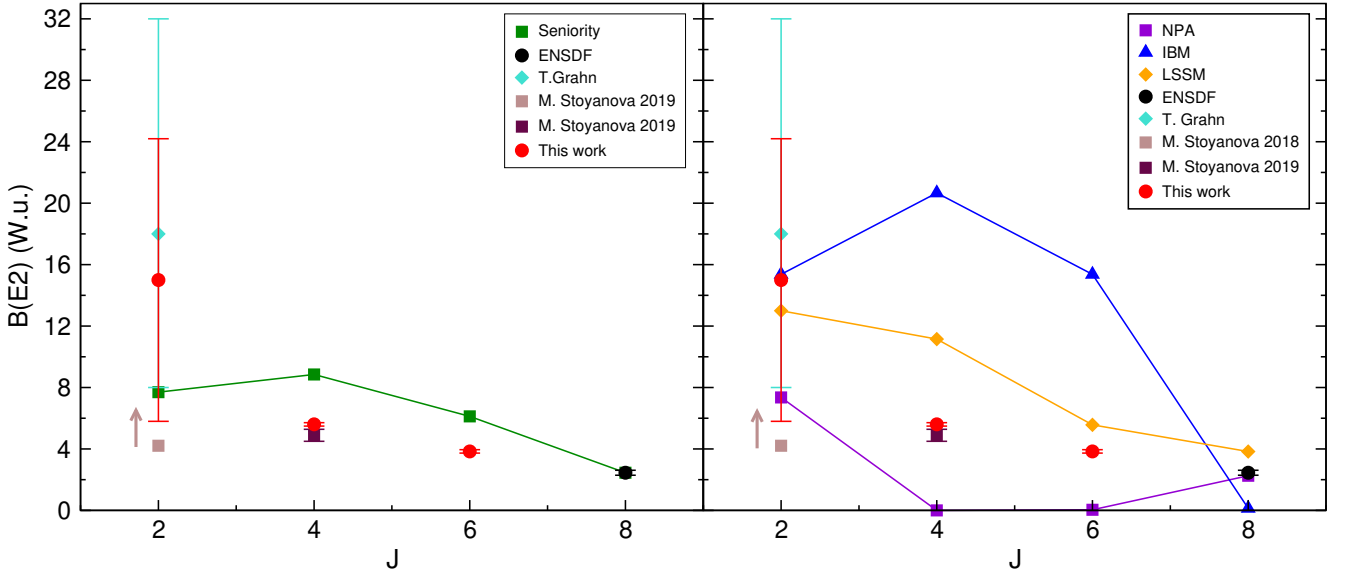


Figure 6.16: Comparison of the experimental values with the theoretical predictions for ^{206}Po .

The values from the two feeding conditions are in agreement. The value I obtained in this analysis for the lifetime of the 6_1^+ state in ^{206}Po is $\tau = 288(8)$ ps. The value of the lifetime was extracted using both the deconvolution method and the slope method. The uncertainty of the lifetime takes into account the statistical uncertainty and accounts for the time-walk difference between the start and the stop energies. With the value of the lifetime, I calculated the value of the reduced transition probability $B(E2; 6_1^+ \rightarrow 4_1^+) = 3.84(11)$ W.u.

The results obtained in this analysis for the ^{206}Po are summarised in Table 6.3. I compared the values obtained in the present analysis with the $B(E2)$ values calculated for a pure j^2 configuration using Eq. 6. This comparison is presented in left panel of Fig. 6.16. In the right panel the results are compared with the available theoretical predictions. One can see that there is a fairly good agreement with the predictions of the simple seniority calculations and with the predictions of LSSM calculations [10], while the predictions of the other theoretical calculation [8, 9] are not in agreement with the experimental data.

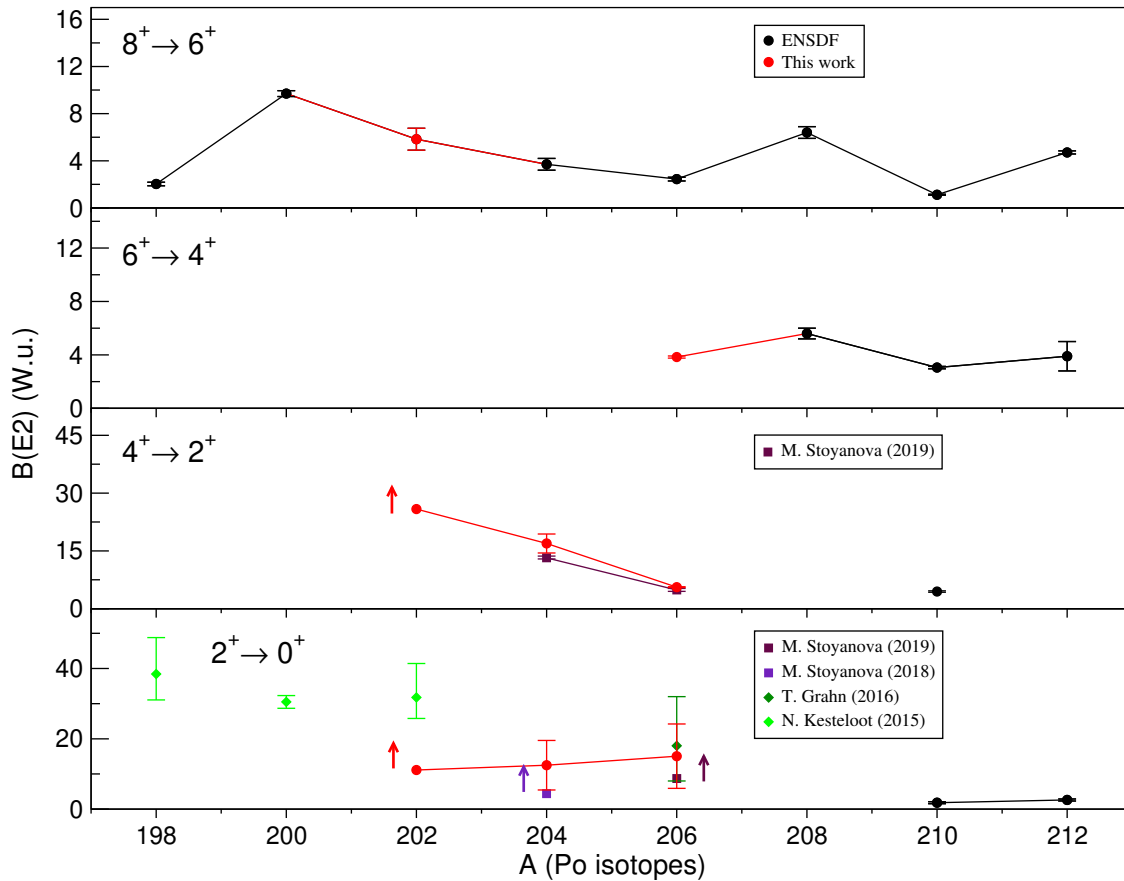


Figure 6.17: Systematics of reduced transition probabilities $B(E2)$ in Polonium isotopes. With red are the results obtained in this work.

Bibliography

- [1] I. Talmi, “Shell model foundations of the interacting boson model,” *Progress in Particle and Nuclear Physics*, vol. 9, pp. 27 – 50, 1983. (Cited on page 1.)
- [2] N. Mărginean *et al.*, “In-beam measurements of sub-nanosecond nuclear lifetimes with a mixed array of HPGe and LaBr3:Ce detectors,” *The European Physical Journal A*, vol. 46, pp. 329–336, Dec 2010. (Cited on pages 2, 8 and 13.)
- [3] T. Grahn *et al.*, “Collective 2_1^+ excitations in ^{206}Po and $^{208,210}\text{Rn}$,” *The European Physical Journal A*, vol. 52, p. 340, Nov 2016. (Cited on page 2.)
- [4] Stoyanova, Milena *et al.*, “A study on the transition between seniority-type and collective excitations in ^{204}Po and ^{206}Po ,” *EPJ Web Conf.*, vol. 194, p. 03002, 2018. (Cited on page 2.)
- [5] M. Stoyanova *et al.*, “Lifetimes of the 4_1^+ states of ^{206}Po and ^{204}Po : A study of the transition from noncollective seniority-like mode to collectivity,” *Phys. Rev. C*, vol. 100, p. 064304, Dec 2019. (Cited on page 2.)
- [6] E. McCutchan, “Evaluated nuclear structure data file.” <https://www.nndc.bnl.gov/ensdf/>. Accessed on 2020-09-25. (Cited on page 2.)
- [7] N. Kesteloot *et al.*, “Deformation and mixing of coexisting shapes in neutron-deficient polonium isotopes,” *Phys. Rev. C*, vol. 92, p. 054301, Nov 2015. (Cited on pages 2 and 19.)
- [8] Z. Y. Xu *et al.*, “Low-lying states of heavy nuclei within the nucleon pair approximation,” *Phys. Rev. C*, vol. 79, p. 054315, May 2009. (Cited on pages 2, 25 and 29.)
- [9] J. E. García-Ramos and K. Heyde, “Nuclear shape coexistence in Po isotopes: An interacting boson model study,” *Phys. Rev. C*, vol. 92, p. 034309, Sep 2015. (Cited on pages 2, 25 and 29.)
- [10] E. Teruya, K. Higashiyama, and N. Yoshinaga, “Large-scale shell-model calculations of nuclei around mass 210,” *Phys. Rev. C*, vol. 93, p. 064327, Jun 2016. (Cited on pages 2 and 29.)
- [11] H. Brown, “A table of relative abundances of nuclear species,” *Rev. Mod. Phys.*, vol. 21, pp. 625–634, Oct 1949. (Cited on page 3.)
- [12] G. Audi, “The history of nuclidic masses and of their evaluation,” *International Journal of Mass Spectrometry*, vol. 251, no. 2, pp. 85 – 94, 2006. ULTRA-ACCURATE MASS SPECTROMETRY AND RELATED TOPICS Dedicated to H.-J. Kluge on the occasion of his 65th birthday anniversary. (Cited on page 3.)
- [13] R. D. Woods and D. S. Saxon, “Diffuse surface optical model for nucleon-nuclei scattering,” *Phys. Rev.*, vol. 95, pp. 577–578, Jul 1954. (Cited on page 3.)
- [14] M. G. Mayer, “On closed shells in nuclei. ii,” *Phys. Rev.*, vol. 75, pp. 1969–1970, Jun 1949. (Cited on page 3.)

- [15] O. Haxel, J. H. D. Jensen, and H. E. Suess, "On the "magic numbers" in nuclear structure," *Phys. Rev.*, vol. 75, pp. 1766–1766, Jun 1949. (Cited on page 3.)
- [16] A. Arima and F. Iachello, *The Interacting Boson Model*, pp. 139–200. Boston, MA: Springer US, 1984. (Cited on page 4.)
- [17] A. Arima and F. Iachello, "Collective Nuclear States as Representations of a SU(6) Group," *Phys. Rev. Lett.*, vol. 35, pp. 1069–1072, Oct 1975. (Cited on page 4.)
- [18] A. Arima and F. Iachello, "Interacting boson model of collective states I. The vibrational limit," *Annals of Physics*, vol. 99, no. 2, pp. 253 – 317, 1976. (Cited on page 4.)
- [19] A. Arima and F. Iachello, "Interacting boson model of collective nuclear states II. The rotational limit," *Annals of Physics*, vol. 111, no. 1, pp. 201 – 238, 1978. (Cited on page 4.)
- [20] O. Scholten, F. Iachello, and A. Arima, "Interacting boson model of collective nuclear states III. The transition from SU(5) to SU(3)," *Annals of Physics*, vol. 115, no. 2, pp. 325 – 366, 1978. (Cited on page 4.)
- [21] A. Arima and F. Iachello, "Interacting boson model of collective nuclear states IV. The O(6) limit," *Annals of Physics*, vol. 123, no. 2, pp. 468 – 492, 1979. (Cited on page 4.)
- [22] Y. Zhao and A. Arima, "Nucleon-pair approximation to the nuclear shell model," *Physics Reports*, vol. 545, no. 1, pp. 1 – 45, 2014. Nucleon-pair approximation to the nuclear shell model. (Cited on page 4.)
- [23] T. Otsuka, M. Honma, T. Mizusaki, N. Shimizu, and Y. Utsuno, "Monte Carlo shell model for atomic nuclei," *Progress in Particle and Nuclear Physics*, vol. 47, no. 1, pp. 319 – 400, 2001. (Cited on page 4.)
- [24] N. Shimizu, T. Abe, Y. Tsunoda, Y. Utsuno, T. Yoshida, T. Mizusaki, M. Honma, and T. Otsuka, "New-generation Monte Carlo shell model for the K computer era," *Progress of Theoretical and Experimental Physics*, vol. 2012, 09 2012. 01A205. (Cited on page 4.)
- [25] M. Honma, T. Mizusaki, and T. Otsuka, "Nuclear shell model by the quantum monte carlo diagonalization method," *Phys. Rev. Lett.*, vol. 77, pp. 3315–3318, Oct 1996. (Cited on page 4.)
- [26] D. Bucurescu *et al.*, "The ROSPHERE γ -ray spectroscopy array," *Nucl. Instrum. Methods Phys. Res. A*, vol. 837, pp. 1 – 10, 2016. (Cited on pages 5, 8, 11, 13 and 14.)
- [27] C. Mihai, *Dezvoltări ale metodelor Doppler de determinare a timpilor de viață nucleari*. PhD thesis, Universitatea din București, Școala Doctorală de Fizică, Bucharest, 2011. (Cited on pages 6, 8 and 10.)
- [28] N. Bohr, "Neutron capture and nuclear constitution," *Nature*, vol. 137, pp. 344 EP –, 02 1936. (Cited on page 6.)

- [29] S. D. Groot, “On the theories of angular distribution and correlation of beta and gamma radiation,” *Physica*, vol. 18, no. 12, pp. 1201 – 1214, 1952. (Cited on page 6.)
- [30] K. Krane, R. Steffen, and R. Wheeler, “Directional correlations of gamma radiations emitted from nuclear states oriented by nuclear reactions or cryogenic methods,” *Atomic Data and Nuclear Data Tables*, vol. 11, no. 5, pp. 351 – 406, 1973. (Cited on page 6.)
- [31] C. N. Pass *et al.*, “Spectroscopic study of sub-barrier quasi-elastic nuclear reactions,” in *Heavy Ion Interactions Around the Coulomb Barrier* (C. Signorini, S. Skorka, P. Spolaore, and A. Vitturi, eds.), (Berlin, Heidelberg), pp. 67–72, Springer Berlin Heidelberg, 1988. (Cited on page 6.)
- [32] M. Macfarlane and J. Schiffer, “IV.B.2 - Transfer reactions.,” in *Nuclear Spectroscopy and Reactions, Part B* (J. CERNY, ed.), vol. 40 of *Pure and Applied Physics*, pp. 169 – 194, Elsevier, 1974. (Cited on page 6.)
- [33] P. J. Nolan and J. F. Sharpey-Schafer, “The measurement of the lifetimes of excited nuclear states,” *Reports on Progress in Physics*, vol. 42, no. 1, p. 1, 1979. (Cited on page 7.)
- [34] P. Regan, “Post graduate nuclear experimental techniques (4NET) course notes,” 2003. (Cited on page 8.)
- [35] D. ALBURGER, “XII - Gamma-radiation from charged particle bombardment; coulomb excitation,” pp. 745 – 768, Amsterdam: Elsevier, 1968. (Cited on page 8.)
- [36] A. Krämer-Flecken, T. Morek, R. Lieder, W. Gast, G. Hebbinghaus, H. Jäger, and W. Urban, “Use of DCO ratios for spin determination in γ – γ coincidence measurements,” *Nucl. Instrum. Methods Phys. Res. A*, vol. 275, no. 2, pp. 333 – 339, 1989. (Cited on page 8.)
- [37] A. Dewald *et al.*, “Electromagnetic transition probabilities in ^{130}Ce ,” *Nuclear Physics A*, vol. 545, no. 4, pp. 822 – 834, 1992. (Cited on pages 9 and 10.)
- [38] G. Böhm, A. Dewald, P. Petkov, and P. von Brentano, “The differential decay curve method for the analysis of Doppler shift timing experiments,” *Nucl. Instrum. Methods Phys. Res. A*, vol. 329, no. 1, pp. 248 – 261, 1993. (Cited on pages 10 and 12.)
- [39] P. Petkov, “Errors arising from nuclear hyperfine interactions on lifetimes determined by the recoil distance Doppler shift method,” *Nucl. Instrum. Methods Phys. Res. A*, vol. 349, no. 1, pp. 289 – 291, 1994. (Cited on page 10.)
- [40] W. Hamilton, ed., *The Electromagnetic Interaction in Nuclear Spectroscopy*. North-Holland, 1975. (Cited on page 13.)
- [41] H. Mach, R. Gill, and M. Moszyński, “A method for picosecond lifetime measurements for neutron-rich nuclei: (1) outline of the method,” *Nucl. Instrum. Methods Phys. Res. A*, vol. 280, no. 1, pp. 49 – 72, 1989. (Cited on page 13.)

- [42] M. Moszyński and H. Mach, “A method for picosecond lifetime measurements for neutron-rich nuclei: (2) timing study with scintillation counters,” *Nucl. Instrum. Methods Phys. Res. A*, vol. 277, no. 2, pp. 407 – 417, 1989. (Cited on page 13.)
- [43] H. Mach *et al.*, “Retardation of $B(E2; 0_1^+ \rightarrow 2_1^+)$ rates in $^{90-96}\text{Sr}$ and strong subshell closure effects in the $A \sim 100$ region,” *Nuclear Physics A*, vol. 523, no. 2, pp. 197 – 227, 1991. (Cited on pages 13 and 14.)
- [44] Z. Bay, “Calculation of decay times from coincidence experiments,” *Phys. Rev.*, vol. 77, pp. 419–419, Feb 1950. (Cited on page 15.)
- [45] C. Wheldon, “Convolution of a gaussian with an exponential (and its application in programs `halflife.c/nanofit.f`.)” http://www.np.ph.bham.ac.uk/research_resources/programs/, October 2014. Accessed on 2019-01-18. (Cited on page 15.)
- [46] C. Qi, L. Y. Jia, and G. J. Fu, “Large-scale shell-model calculations on the spectroscopy of $N < 126$ Pb isotopes,” *Phys. Rev. C*, vol. 94, p. 014312, Jul 2016. (Cited on page 18.)
- [47] A. E. Stuchbery, “Gyromagnetic ratios of excited states and nuclear structure near 132sn ,” *AIP Conference Proceedings*, vol. 1625, no. 1, pp. 52–58, 2014. (Cited on page 22.)